International Journal of Mechanical System Dynamics

WILEY

IJMSD International Journal of Mechanical System Dynamics Open Access

RESEARCH ARTICLE OPEN ACCESS

Robust Control for Uncertain Vertical Electric Stabilization System With Flexible Nonlinearity Using Backstepping Idea

Peng Liu | Tan Lu | He Zhang

School of Mechanical Engineering, Nanjing University of Science and Technology, Nanjing, China

Correspondence: Peng Liu (njustca@njust.edu.cn)

Received: 20 January 2025 | **Revised:** 25 March 2025 | **Accepted:** 9 April 2025

Keywords: backstepping idea | flexible nonlinearity | mismatched uncertainty | robust control | vertical electric stabilization system

ABSTRACT

A robust control method for the uncertain vertical electric stabilization system (VESS) with flexible nonlinearity is proposed, and the mismatched uncertainty is considered and compensated based on the backstepping idea. First, based on evaluating the coupling effects of the flexible nonlinearity, the analytical dynamics model of the VESS is established. Second, the tracking error is defined as the evaluation of the system's pitch-pointing tracking control, and then the mismatched state space model with two interconnected subsystems is established as the controlled system. Third, the original mismatched system is converted to the locally matched system using the backstepping design to transform the system state variables. The robust control is proposed to handle the flexible nonlinearity and mismatched uncertainty, which can make both the original system and the reconfigured system present practical stability. Finally, the effectiveness of the proposed control is verified by numerical simulation experiments. This study should be the first to consider flexible nonlinearity coupling and two different uncertainties (matched and mismatched uncertainty) in the design of pitch-pointing tracking control for the vertical electric stabilization system (VESS).

1 | Introduction

To enhance survival and combat effectiveness on the battlefield, modern tanks are designed with an emphasis on lightness and speed. However, this design approach often leads to increased hull vibration [1], which exacerbates the impact of flexible nonlinearity on the tank pitch-pointing tracking control [2, 3]. Given that the mechanical structure of the tank vertical electric stabilization system (VESS) primarily consists of the actuator (electric cylinder) and the load mechanism (barrel), a comprehensive analysis of the flexible characteristics of both the electric cylinder and the barrel is essential for improving the pitch-pointing tracking control performance of modern tanks.

As a critical component of modern tank fire control systems, the control performance of the VESS directly influences the accuracy and hit rate of tank firing [4, 5]. In recent years, significant research has been conducted to analyze the coupling relationships among the servo motor, gearbox, ball screw system, and control system of the VESS. Novel control algorithms have been proposed to enhance pitch-pointing tracking control [6–8]. However, these studies primarily focus on addressing friction nonlinearity, gear backlash nonlinearity, and damping nonlinearity, while largely neglecting the flexible nonlinearity. This oversight limits the ability to meet control requirements under strong vibration conditions, which are common in battlefield scenarios. To address this gap, we constructed an analytical dynamics

Abbreviations: ANA, anti-nuclear antibodies; APC, antigen-presenting cells; IRF, interferon regulatory factor.

model of the VESS that incorporates flexible nonlinearity by developing an axial stiffness model for the electric cylinder and a modal solution for the flexible barrel. Through the fine modeling of the VESS, the adverse effects of flexible nonlinearity can be suppressed.

In fact, for the controller design of the system, strong nonlinear factors and complex uncertainties inevitably increase the complexity of the control process. In a general electromechanical servo system, uncertainty includes matched and mismatched uncertainty. The matched uncertainty is located in the parameter space of the control matrix and can be compensated for directly by adjusting the control input. In contrast, the mismatched uncertainty exists outside the parameter space of the control matrix and cannot be solved directly by adjusting the control input [9, 10]. Most of the pitch-point tracking control strategies used for VESS focus on compensating for the matched uncertainty [11–13], but the research on the mismatched uncertainty is limited, which can reduce the difficulty of controller design. However, the unmodeled dynamics of the VESS are easily excited by the strong robustness of the controller to suppress the mismatched uncertainty, which leads to the instability of the VESS. Given the inherent complex and flexible nonlinearity of the system, it is important to solve the problem of mismatch uncertainty to meet the requirements of control design. To address this challenge, we construct a state-space model of controlled systems with mismatched uncertainties based on the analytical dynamics model of VESS.

Many advanced control algorithms have been developed to address system uncertainties and nonlinearities, including adaptive robust control [14–16], sliding mode control [17, 18], adaptive state-constrained control [19, 20], event-triggered control [21–23], Lyapunov-based control [24–26], and intelligent control [27–29]. The above controller provides a systematic reference for the control algorithm design of high-end equipment, and can be integrated and optimized according to specific working conditions in practical applications. Moreover, in dealing with flexible nonlinearity, Xu [30] proposed a singular perturbation theory-based composite learning control for flexible-link manipulators, while Yang et al. [31] investigated trajectory tracking and vibration reduction in flexible manipulators using an adaptive control method with an iterative learning scheme. For mismatched uncertainty, Chen [32] introduced a novel control algorithm that characterizes the structure of uncertainty in mismatched systems, and Xu et al. [33] developed a fuzzy-based optimal approach for robust control design in interconnected uncertain systems with mismatched conditions. Additionally, Sun et al. [34] designed a robust controller to handle both matched and mismatched uncertainties in vertical electrohydraulic stabilization systems. Despite the advancements in control strategies for VESS, existing methods often fail to simultaneously address flexible nonlinearity and mismatched uncertainty, which are critical challenges in tank gun control systems. This gap motivates the development of a novel control approach that can effectively handle both issues while ensuring practical stability and high tracking accuracy. Building on these advancements, this paper adopts the backstepping design approach to transform the system state variables, converting the original uncertain system into a locally matched uncertainty system. Subsequently, a robust control method is proposed to address the flexible nonlinearity and mismatched uncertainty, ensuring practical stability for both the original and reconfigured systems.

In this paper, the flexible nonlinearity of the system is characterized through nonlinear mechanism functions, which are integrated into the analytical dynamics model. The mismatched state space model is developed to address the mismatched uncertainty, providing a foundation for subsequent controller design. Meanwhile, the original mismatched uncertain system is transformed into a locally matched uncertain system by redefining the system state variables. Furthermore, a robust control method is proposed to effectively handle both mismatched uncertainty and flexible nonlinearity, ensuring practical stability for both the original and reconfigured systems. Finally, simulation and experimental results demonstrate that the proposed control method outperforms existing approaches in terms of accuracy, robustness, and stability. The primary innovation of this study lies in the simultaneous consideration of flexible nonlinear coupling and two types of uncertainties (matched and mismatched) in the pitch-pointing tracking control design for the vertical electric stabilization system (VESS). Unlike existing methods that typically focus on either matched uncertainties or specific types of nonlinearities (e.g., friction or gear backlash), our approach addresses the complex interplay between flexible nonlinearity and mismatched uncertainty, which is particularly critical in applications such as tank gun control systems. This comprehensive treatment enables superior control performance under strong vibration conditions, where traditional methods often fall short.

The main contributions of this study are threefold: (1) the first integration of flexible nonlinear coupling and mismatched uncertainty into the pitch-pointing tracking control design for VESS; (2) the development of a mismatched state space model and its transformation into a locally matched system using backstepping design; and (3) the proposal of a robust control method that ensures practical stability for both the original and reconfigured systems. These innovations provide a comprehensive solution to the challenges posed by flexible nonlinearity and mismatched uncertainty in high-vibration environments.

2 | System Modeling: Flexible Nonlinearity and Dynamics of VESS

2.1 | Axial Stiffness Model of the Electric Cylinder

As an essential part of the VESS, the flexible deformation of the electric cylinder has a significant impact on the system stability and control performance. Considering that axial deformation is the main influencing factor, the focus of this paper is to construct the axial stiffness model of the electric cylinder. As shown in Figure 1, the servo electric cylinder in VESS is mainly composed of servo motor, gearbox, bearing set, ball screw, and pushrod.

The total axial stiffness of the electric cylinder is the series sum of the stiffness of each component, among which the axial

stiffness of the bearing set, screw, nut, and pushrod has the most significant influence, and the influence of other parts is small and negligible. From the axial stiffness model of the bearing set, screw, nut, and pushrod [35], it is known that the axial stiffness of the servo-electric cylinder k_{se} is not only related to the structural size and material performance parameters of the electric cylinder, but also proportional to the one-third power of the axial load size. Considering the small change of the electric cylinder output force size when the tank VESS is working, the axial stiffness of the electric cylinder can be regarded as the system uncertainty, the nominal part of which is constant value and independent of the axial load size, the uncertainty part may change rapidly with time, but bounded.

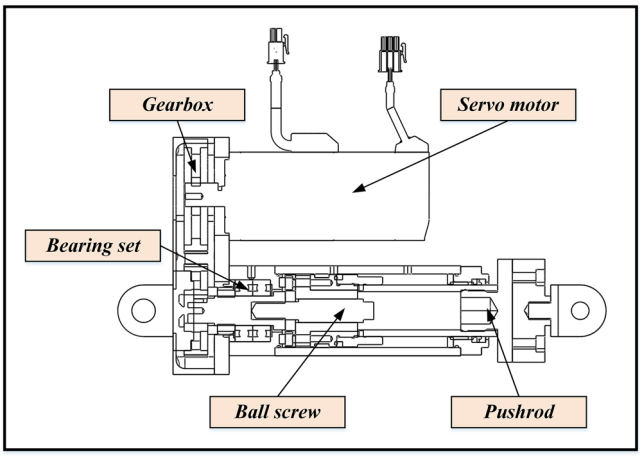

FIGURE 1 | The structure schematic diagram of the servo electric cylinder.

2.2 | Modal Solution of Flexible Barrel

The tank barrel is a kind of tubular flexible structure using gun steel as the material, and its Schematic diagram is shown in Figure 2. The tail end of the barrel is connected with the cradle and the gun breech to form the load unit of the VESS. The length of the restrained section of the barrel L_1 is the distance between the gun breech and the trunnion center point, and the length of the unrestrained section of the barrel L_2 is the distance between the muzzle and the trunnion center point. Considering that the bending deformation of the flexible barrel is much larger than its shear deformation and axial deformation, it is simplified as the Euler-Bernoulli beam in Figure 3, only considering its bending deformation and ignoring its shear deformation and axial deformation, and the structure stiffness of the gun breech and cradle is larger, so the flexible deformation of the restrained section of the barrel L_1 is smaller and can be ignored. In Figure 3, OXY is the inertial coordinate system, Oxy is the floating coordinate system fixed on the barrel, O is the center point of the trunnion, m is the mass of the load unit, ρ is the density of the flexible barrel, A is the cross-sectional area of the barrel, EI is the flexural stiffness of the flexible barrel, where E is the modulus of elasticity, I is the moment of inertia of the cross-section, the barrel does pitching motion around the center point of the trunnion under the action of the moment T, $\varphi(t)$ is the pitch angle at the cradle measured by the gyroscope at the trunnion, $\varphi_r(t)$ is the pitch angle of the barrel, $\delta(x, t)$ is the flexible deformation in the process of motion due to the flexibility of the barrel at x. By geometric relationship, we have

$$y(x, t) = \varphi(t)x + \delta(x, t), \tag{1}$$

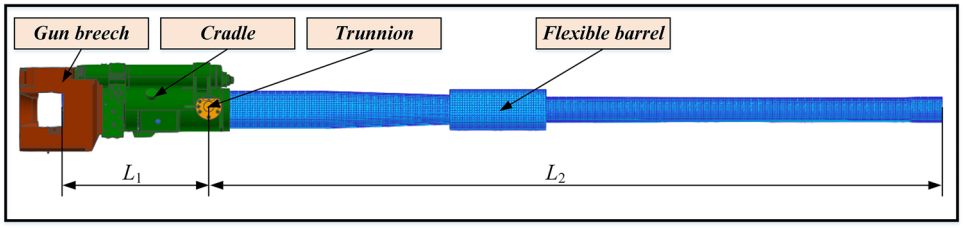

FIGURE 2 | Schematic diagram of flexible barrel.

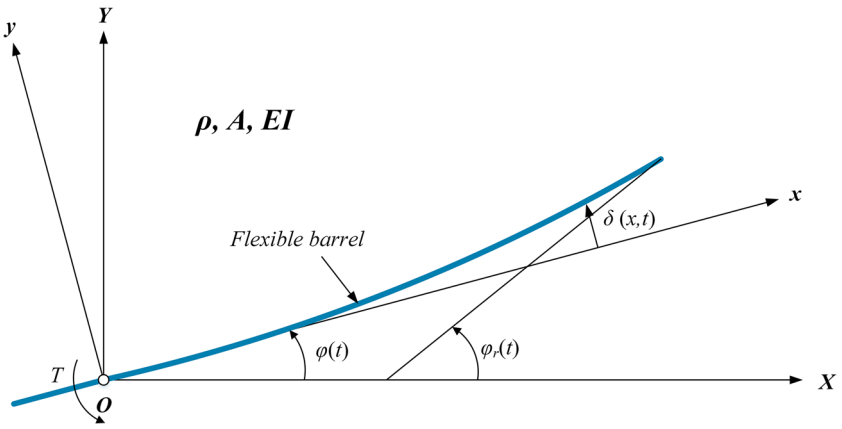

FIGURE 3 | Physical model of flexible barrel.

$$\varphi_r(t) = \varphi(t) + \frac{\partial \delta(L_2, t)}{\partial x}, \tag{2}$$

where $y(x, t)$ is the displacement of the barrel.

According to the hypothetical modal method, the deformation of the barrel at moment t during the motion can be described as

$$\delta(x, t) = \sum_{i=1}^{\infty} \phi_i(x) h_i(t), \tag{3}$$

where $\phi_i(x)$ denotes the ith order vibration function, and $h_i(t)$ denotes the corresponding modal coordinates. Considering the small vibration amplitude of the higher-order modals of the flexible barrel, this paper mainly studies the influence of the bending deformation of the flexible barrel on the control performance of the system, to simplify the research process, only the first-order modal of the barrel is considered, and the influence of the remaining modals on the system can be neglected, that is

$$\delta(x, t) \approx \phi_1(x) h_1(t). \tag{4}$$

Considering the small change in the cross-sectional area of the barrel and the overall use of the same material, the unrestrained section of the barrel can be regarded as a homogeneous beam of equal cross-section with one end fixed and one end free (cantilever beam), from which the boundary conditions can be determined, and the specific expression of the vibration function $\phi_i(x)$ is [36]

$$\phi_i(x) = \cosh \beta_i^E x - \cos \beta_i^E x + \xi_i \left(\sinh \beta_i^E x - \sin \beta_i^E x \right), \tag{5}$$

where $\xi_i = -\frac{\cosh \beta_i^E L_2 + \cos \beta_i^E L_2}{\sinh \beta_i^E L_2 + \sin \beta_i^E L_2}$, β_i^E can be obtained from the following equation:

$$\cos(\beta^E L_2) \cosh(\beta^E L_2) = -1. \tag{6}$$

According to the initial vibration conditions of the flexible barrel, the expressions for the inherent frequency and modal coordinates of the flexible barrel are

$$\omega_i = \left(\beta_i^E\right)^2 \sqrt{\frac{EI}{\rho A}}, \tag{7}$$

$$h_i(t) = \sin \omega_i t. \tag{8}$$

With the flexible nonlinearity of the system characterized, the next step is to develop a dynamical model that incorporates both matched and mismatched uncertainties. In Section 2.3, we construct a mismatched state space model of the VESS, which serves as the foundation for the subsequent controller design.

2.3 | Dynamical Model of the Uncertain VESS

The tank VESS is mainly composed of a motor, a flexible electric cylinder, and a flexible barrel, and its multibody model is shown in Figure 4, in which the finite element mesh cell is taken to characterize the flexible characteristics of the uncertain system.

The output torque of the motor is amplified by the gearbox to drive the ball screw of the electric cylinder to rotate, the screw nut, which is limited in the radial direction, is driven by the rotating force of the screw to do linear motion together with the pushrod, and the pushrod of the electric cylinder applies thrust at point O_1 of the barrel to drive the load to rotate around the center point of the trunnion for meeting the angle adjustment command of the fire control system. The simplified schematic diagram of the system mechanics is shown in Figure 5, where O_2 is the center of gravity of the load, θ_0 is the initial angle of the electric cylinder, d_0 is the initial length of the electric cylinder, $d_1(t)$ is the theoretical working length of the electric cylinder, $d_f(t)$ is the axial flexible deformation of the electric cylinder, l_1 and l_2 are the lengths of the segment OO_1 and segment OO_2, respectively, l_3 is the distance from the upper pivot of the electric cylinder to the center point of the trunnion, and $F(t)$ is the thrust of the electric

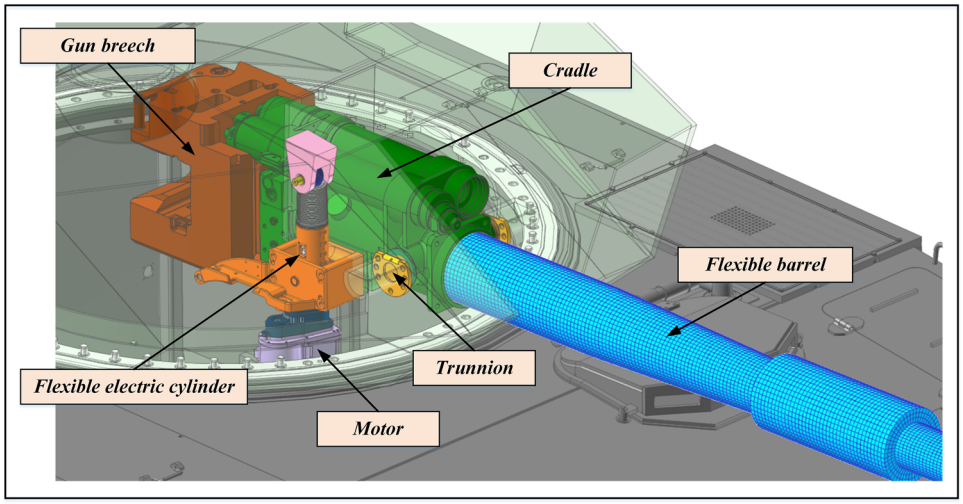

FIGURE 4 | Multibody model of the VESS.

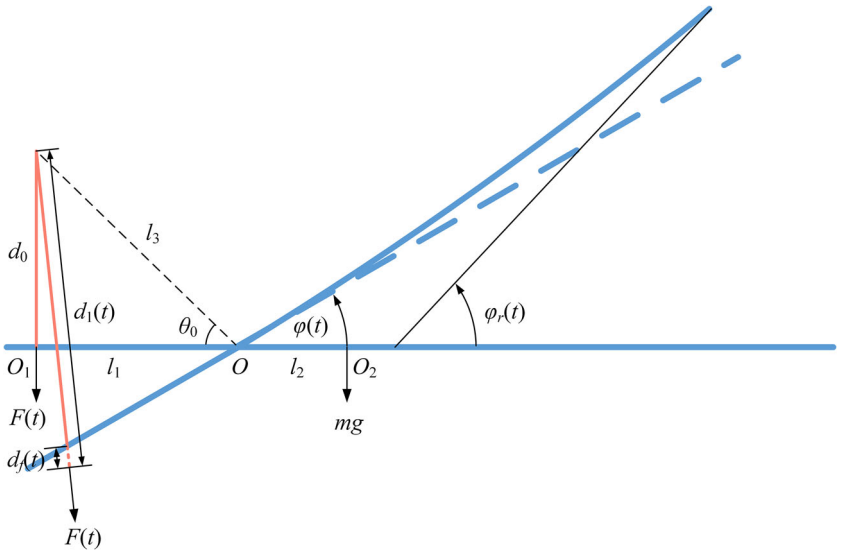

FIGURE 5 | Simplified schematic diagram of the system mechanics.

cylinder. Based on the working principle of motor-gearbox system, the dynamics model can be expressed as

$$T_m(t) = \frac{ik_t}{R}u(t) - i^2 J_m \ddot{\varphi}_m(t) - \frac{i^2 k_t k_e}{R}\dot{\varphi}_m(t) - i^2 B_m \dot{\varphi}_m(t), \tag{9}$$

where $T_m(t)$ is the output torque of motor-gearbox system, i is the gear ratio, $u(t)$ is the control input voltage, k_t and k_e are the motor torque constant and the electromotive force constant, respectively. J_m and B_m are the moments of inertia and viscous damping coefficients of the motor, $\varphi_m(t)$ is the angular displacement of the motor-gearbox system, and R is the total resistance of the armature circuit.

According to the working principle of electric cylinder system, the dynamics model of ball screw can be expressed as

$$F(t) = \frac{2\pi}{P_h}[T_m(t) - J_b \ddot{\varphi}_m(t) - B_b \dot{\varphi}_m(t)], \tag{10}$$

$$\Delta d(t) = d_1(t) - d_0 = \frac{P_h}{2\pi}\varphi_m(t), \tag{11}$$

$$d_f(t) = \frac{F(t)}{k_{se}}, \tag{12}$$

where P_h, J_b, and B_b are the lead, the moments of inertia, and the viscous damping coefficients of ball-screw, $\Delta d(t)$ is the theoretical displacement of the screw.

For the load unit of the VESS rotating around the center point of the trunnion, the total kinetic energy can be expressed as

$$\begin{aligned} T &= \frac{1}{2}\int_0^{L_2} \rho A \left[\frac{\partial y(x,t)}{\partial t}\right]^2 \mathrm{d}x \\ &= \frac{1}{6}mL_2^2\dot{\varphi}^2(t) + \rho A\dot{\varphi}(t)\dot{h}(t)\int_0^{L_2} x\phi(x)\mathrm{d}x \\ &\quad + \frac{1}{2}\rho A\dot{h}^2(t)\int_0^{L_2}\phi^2(x)\mathrm{d}x. \end{aligned} \tag{13}$$

The total potential energy can be expressed as

$$\begin{aligned} U &= \int_0^{L_2} \rho A g x \sin\varphi(t)\mathrm{d}x + \frac{1}{2}\int_0^{L_2} EI\left[\frac{\partial^2\delta(x,t)}{\partial x^2}\right]^2 \mathrm{d}x \\ &= \frac{1}{2}mgL_2\sin\varphi(t) + \frac{1}{2}EIh^2(t)\int_0^{L_2}\ddot{\phi}^2(x)\mathrm{d}x. \end{aligned} \tag{14}$$

The Euler-Lagrange equations of the flexible barrel are

$$\frac{\mathrm{d}}{\mathrm{d}t}\frac{\partial L}{\partial \dot{\boldsymbol{q}}} - \frac{\partial L}{\partial \boldsymbol{q}} = \boldsymbol{Q}, \tag{15}$$

where $L = T - U$ is the Lagrangian, $\boldsymbol{q} = (\varphi, h)^{\mathrm{T}} \in \mathbf{R}^2$ is the generalized coordinates, and $\boldsymbol{Q} = (F(t)l_1, 0)^{\mathrm{T}} \in \mathbf{R}^2$ is the generalized force. The computation of Equation (15) results in the following equations:

$$\begin{cases} \frac{1}{3}mL_2^2\ddot{\varphi}(t) + \rho A\ddot{h}(t)\int_0^{L_2} x\phi(x)\mathrm{d}x + \frac{1}{2}mgL_2\cos\varphi(t) \\ \qquad + f_d(t) = F(t)l_1, \\ \rho A\ddot{\varphi}(t)\int_0^{L_2} x\phi(x)\mathrm{d}x + \rho A\ddot{h}(t)\int_0^{L_2}\phi^2(x)\mathrm{d}x \\ \qquad + EIh(t)\int_0^{L_2}\ddot{\phi}^2(x)\mathrm{d}x = 0, \end{cases} \tag{16}$$

where $f_d(t) \in \mathbf{R}$ is the external disturbance torque mainly caused by the road excitation. Equation (16) can be further rewritten as

$$\ddot{\varphi}(t) = \frac{F(t)l_1 - \frac{1}{2}mgL_2\cos\varphi(t) + EIK_n h(t) - f_d(t)}{\frac{1}{3}mL_2^2 - \rho AK_m}, \tag{17}$$

where $K_m = \frac{\left(\int_0^{L_2} x\phi(x)\mathrm{d}x\right)^2}{\int_0^{L_2}\phi^2(x)\mathrm{d}x}$ and $K_n = \frac{\int_0^{L_2} x\phi(x)\mathrm{d}x \times \int_0^{L_2}\ddot{\phi}^2(x)\mathrm{d}x}{\int_0^{L_2}\phi^2(x)\mathrm{d}x}$. Here, K_m and K_n are coefficients related to the flexible barrel's modal characteristics. K_m represents the influence of the barrel's bending deformation on the system dynamics, while K_n captures the coupling effect between the barrel vibration and the system's motion.

According to the geometric relationship in Figure 5, then

$$d_1(t) - d_f(t) = \left(l_1^2 + l_3^2 - 2l_1 l_3 \cos(\varphi(t) + \theta_0)\right)^{\frac{1}{2}}, \quad (18)$$

with Equations (11), (12), and (18):

$$\varphi_m(t) = \frac{2\pi}{P_h}\left[\left(l_1^2 + l_3^2 - 2l_1 l_3 \cos(\varphi(t) + \theta_0)\right)^{\frac{1}{2}} - d_0\right] + \frac{2\pi}{P_h k_{se}} F(t). \quad (19)$$

$$\begin{cases} \ddot{\varphi}(t) = \dfrac{l_1}{C_1}F(t) - \dfrac{mgL_2}{2C_1}\cos\varphi(t) + \dfrac{EIK_n}{C_1}h(t) - \dfrac{1}{C_1}f_d(t), \\ \ddot{F}(t) = \dfrac{ik_tP_h}{2\pi RJ_{eq}}k_{se}u(t) + \left(l_1^2 l_3^2 K_a^3 K_b^2 - l_1 l_3 K_a K_c\right)k_{se}\dot{\varphi}^2(t) \\ \quad - \dfrac{l_1 l_3 B_{eq} K_a K_b}{J_{eq}}k_{se}\dot{\varphi}(t) - \dfrac{i^2 k_t k_e l_1 l_3 K_a K_b}{RJ_{eq}}k_{se}\dot{\varphi}(t) \\ \quad + \dfrac{mgL_2 l_1 l_3 K_a K_b}{2C_1}k_{se}\cos\varphi(t) - \dfrac{RB_{eq} + i^2 k_t k_e}{RJ_{eq}}\dot{F}(t) \\ \quad - \dfrac{P_h^2}{4\pi^2 J_{eq}}k_{se}F(t) - \dfrac{l_1^2 l_3 K_a K_b}{C_1}k_{se}F(t) \\ \quad - \dfrac{l_1 l_3 EIK_n K_a K_b}{C_1}k_{se}h(t) + \dfrac{l_1 l_3 K_a K_b}{C_1}k_{se}f_d(t). \end{cases} \quad (20)$$

where

$$\begin{aligned} C_1 &= \frac{1}{3}mL_2^2 - \rho AK_m, \quad J_{eq} = (i^2 J_m + J_b), \\ B_{eq} &= (i^2 B_m + B_b), \\ K_a &= \left(l_1^2 + l_3^2 - 2l_1 l_3 \cos(\varphi(t) + \theta_0)\right)^{-\frac{1}{2}}, \\ K_b &= \sin(\varphi(t) + \theta_0), \quad K_c = \cos(\varphi(t) + \theta_0). \end{aligned} \quad (21)$$

Based on the dynamical model of the uncertain VESS, the next step is to formulate the pitch-pointing tracking problem. In Section 3, we define the tracking error and establish the control objectives, laying the groundwork for the design of the robust backstepping controller in Section 4.

3 | Formulation of Pointing Tracking Problem for the VESS

The main function of the VESS is to achieve real-time pitch-pointing tracking of the tank to the enemy target, so the goal of the tank vertical stabilization control is to design the controller so that the pitch angle of the barrel is maintained at the target angle. Thus, the tank pitch-pointing tracking control can be converted into a class of problems that induce the pitch angle of barrel $\varphi_r(t)$ to track the desired reference signal $\varphi_d(t)$ approximately, while enabling the controlled system to suppress uncertainty interference during the signal tracking process autonomously. Assume that $\varphi_d(\cdot) : [t_0, \infty] \to \mathbf{R}$ is a second-order differentiable signal function, and $\varphi_d, \dot{\varphi}_d$ are uniformly bounded. The tracking error $e(t)$ is thus defined as

$$e(t) = \varphi_r(t) - \varphi_d(t). \quad (22)$$

Taking Equations (2) and (4) into Equation (22):

$$e(t) = \varphi(t) + \dot{\phi}(L_2)h(t) - \varphi_d(t). \quad (23)$$

Then

$$\begin{aligned} \varphi(t) &= e(t) - \dot{\phi}(L_2)h(t) + \varphi_d(t), \\ \dot{\varphi}(t) &= \dot{e}(t) - \dot{\phi}(L_2)\dot{h}(t) + \dot{\varphi}_d(t), \\ \ddot{\varphi}(t) &= \ddot{e}(t) - \dot{\phi}(L_2)\ddot{h}(t) + \ddot{\varphi}_d(t). \end{aligned} \quad (24)$$

Let $\boldsymbol{x}_1 \coloneqq [x_{11}, x_{12}]^{\mathrm{T}} = [e(t), \dot{e}(t)]^{\mathrm{T}}$ and $\boldsymbol{x}_2 \coloneqq [x_{21}, x_{22}]^{\mathrm{T}} = [F(t), \dot{F}(t)]^{\mathrm{T}}$, substitute it into Equation (24):

$$\begin{aligned} \varphi(t) &= x_{11}(t) - \dot{\phi}(L_2)h(t) + \varphi_d(t), \\ \dot{\varphi}(t) &= x_{12}(t) - \dot{\phi}(L_2)\dot{h}(t) + \dot{\varphi}_d(t), \\ \ddot{\varphi}(t) &= \dot{x}_{12}(t) - \dot{\phi}(L_2)\ddot{h}(t) + \ddot{\varphi}_d(t). \end{aligned} \quad (25)$$

substitute Equation (25) into Equation (20):

$$\begin{aligned} \dot{x}_{12} &= \frac{l_1}{C_1}x_{21} - \frac{mgL_2}{2C_1}\cos[x_{11} - \dot{\phi}(L_2)h + \varphi_d] \\ &\quad + \frac{EIK_n}{C_1}h - \frac{1}{C_1}f_d + \dot{\phi}(L_2)\ddot{h} - \ddot{\varphi}_d, \\ \dot{x}_{22} &= \frac{ik_tP_h}{2\pi RJ_{eq}}k_{se}u + k_{se}S(x_{11}, x_{12}, x_{21}) \\ &\quad - \frac{RB_{eq} + i^2k_tk_e}{RJ_{eq}}x_{22} + \frac{l_1 l_3 K_a K_b}{C_1}k_{se}f_d, \end{aligned} \quad (26)$$

with the definitions

$$\begin{aligned} S(x_{11}, x_{12}, x_{21}, t) &= \left(l_1^2 l_3^2 K_a^3 K_b^2 - l_1 l_3 K_a K_c\right)\left[x_{12} - \dot{\phi}(L_2)\dot{h} + \dot{\varphi}_d\right]^2 \\ &\quad - \frac{l_1 l_3 B_{eq} K_a K_b}{J_{eq}}\left[x_{12} - \dot{\phi}(L_2)\dot{h} + \dot{\varphi}_d\right] \\ &\quad - \frac{i^2 k_t k_e l_1 l_3 K_a K_b}{RJ_{eq}}\left[x_{12} - \dot{\phi}(L_2)\dot{h} + \dot{\varphi}_d\right] \\ &\quad + \frac{mgL_2 l_1 l_3 K_a K_b}{2C_1} \times \cos\left[x_{11} - \dot{\phi}(L_2)h + \varphi_d\right] \\ &\quad - \frac{P_h^2}{4\pi^2 J_{eq}}x_{21} - \frac{l_1^2 l_3 K_a K_b}{C_1}x_{21} \\ &\quad - \frac{l_1 l_3 EIK_n K_a K_b}{C_1}h. \end{aligned} \quad (27)$$

Consider the axial stiffness of the electric cylinder k_{se} and the external disturbance torque f_d as the uncertainties in the VESS (26) with flexible nonlinearity, and decompose them into nominal and uncertain portions as

$$k_{se} = \bar{k}_{se} + \Delta k_{se}, \quad f_d = \bar{f}_d + \Delta f_d, \tag{28}$$

where $\bar{k}_{se}$ and $\bar{f}_d$ are the nominal portions, Δk_{se} and Δf_d are the uncertain portions, which are possibly fast time varying but bounded, and the bounds can be described as

$$|\Delta k_{se}| \le \hat{k}_{se}, |\Delta f_d| \le \hat{f}_d. \tag{29}$$

Remark 1. Considering that unbounded uncertainty requires infinite energy to be maintained, any parameter with physical significance and its uncertainty part is bounded. Besides, the nominal part of the parameter with uncertainty is usually chosen based on engineering experience, so it is always known as well.

Let $\boldsymbol{\sigma} := [\sigma_1, \sigma_2]^{\mathrm{T}} = [\Delta f_d, \Delta k_{se}]^{\mathrm{T}}$ be the uncertain portions of the system; by introducing the decompositions of k_{se} and f_d into the uncertain system (26) and classifying the system as the nominal and uncertain portions, Equation (26) can be re-written as

$$\begin{aligned} \dot{x}_{12} &= \bar{g}_{12} + \Delta g_{12} + P_{21} x_{21}, \\ \dot{x}_{22} &= \bar{g}_{22} + \Delta g_{22} + (B_{21} + \Delta B_{21}) u, \end{aligned} \tag{30}$$

with the definitions of

$$\begin{aligned} \Delta g_{12}(x_{11}, x_{12}, t) &= -\frac{1}{C_1}\Delta f_d + Z_1(x_{11}, x_{12}, t) - \bar{g}_{12}, \\ Z_1(x_{11}, x_{12}, t) &= -\frac{mgL_2}{2C_1}\cos\left[x_{11} - \dot{\phi}(L_2)h + \varphi_d\right] \\ &\quad + \frac{EIK_n}{C_1}h - \frac{1}{C_1}\bar{f}_d + \dot{\phi}(L_2)\ddot{h} - \ddot{\varphi}_d, \\ P_{21} &= \frac{l_1}{C_1}, \\ \Delta g_{22}(x_{11}, x_{12}, x_{21}, x_{22}, t) &= \Delta k_{se} S(x_{11}, x_{12}, x_{21}, t) + \frac{l_1 l_3 K_a K_b}{C_1} \\ &\quad \times (\Delta k_{se}\bar{f}_d + \bar{k}_{se}\Delta f_d + \Delta k_{se}\Delta f_d) \\ &\quad + Z_2(x_{11}, x_{12}, x_{21}, t) + g_{22} - \bar{g}_{22}, \\ Z_2(x_{11}, x_{12}, x_{21}, t) &= \bar{k}_{se} S(x_{11}, x_{12}, x_{21}, t) \\ &\quad + \frac{l_1 l_3 K_a K_b}{C_1}\bar{k}_{se}\bar{f}_d, \\ g_{22}(x_{11}, x_{12}, x_{21}, x_{22}, t) &= -\frac{RB_{eq} + i^2 k_t k_e}{RJ_{eq}} x_{22}, \\ B_{21} &= \frac{ik_t P_h}{2\pi R J_{eq}}\bar{k}_{se}, \\ \Delta B_{21}(\sigma_1, t) &= \frac{ik_t P_h}{2\pi R J_{eq}}\Delta k_{se}. \end{aligned} \tag{31}$$

where $\bar{g}_{12}(\cdot)$ is a function of x_{11}, x_{12} and t, and $\bar{g}_{22}(\cdot)$ is a function of x_{21}, x_{22} and t.

As a result, the VESS with flexible nonlinearity can be described as a coupling system in a state-space form as

$$\begin{aligned} (N_1)\dot{\boldsymbol{x}}_1(t) &= \begin{bmatrix} x_{12}(t) \\ \bar{g}_{12}(x_{11}(t), x_{12}(t), t) \end{bmatrix} \\ &\quad + \begin{bmatrix} 0 \\ \Delta g_{12}(x_{11}(t), x_{12}(t), \sigma_1(t), t) \end{bmatrix} + \begin{bmatrix} 0 & 0 \\ P_{21} & 0 \end{bmatrix}\begin{bmatrix} x_{21} \\ x_{22} \end{bmatrix} \\ &= \boldsymbol{g}_1(\boldsymbol{x}_1(t), t) + \Delta \boldsymbol{g}_1(\boldsymbol{x}_1(t), \boldsymbol{\sigma}(t), t) + \boldsymbol{P}\boldsymbol{x}_2(t), \\ (N_2)\dot{\boldsymbol{x}}_2(t) &= \begin{bmatrix} x_{22}(t) \\ \bar{g}_{22}(x_{21}(t), x_{22}(t), t) \end{bmatrix} \\ &\quad + \begin{bmatrix} 0 \\ \Delta g_{22}(x_{11}(t), x_{12}(t), x_{21}(t), x_{22}(t), \sigma_1(t), \sigma_2(t), t) \end{bmatrix} \\ &\quad + \left(\begin{bmatrix} 0 \\ B_{21} \end{bmatrix} + \begin{bmatrix} 0 \\ \Delta B_{21}(\sigma_1(t), t) \end{bmatrix}\right) u(t) \\ &= \boldsymbol{g}_2(\boldsymbol{x}_2(t), t) + \Delta \boldsymbol{g}_2(\boldsymbol{x}_1(t), \boldsymbol{x}_2(t), \boldsymbol{\sigma}(t), t) \\ &\quad + (\boldsymbol{B} + \Delta \boldsymbol{B}(\boldsymbol{\sigma}(t), t)) u(t), \end{aligned} \tag{32}$$

where $t \in \mathbf{R}$ is the time, $\boldsymbol{x}_1(t), \boldsymbol{x}_2(t) \in \mathbf{R}^2$ are the system state variable, $u(t) \in \mathbf{R}$ is the servo motor control input, $\boldsymbol{\sigma}(t) \in \Sigma \subset \mathbf{R}^2$ is the system uncertain parameter, $\Sigma \subset \mathbf{R}^2$ is unknown compact, which stands for the possible boundary of Σ. Besides, $\boldsymbol{g}_1(\boldsymbol{x}_1(t), t)$, $\Delta \boldsymbol{g}_1(\boldsymbol{x}_1(t), \boldsymbol{\sigma}(t), t)$, $\boldsymbol{P}$, $\boldsymbol{g}_2(\boldsymbol{x}_2(t), t)$, $\Delta \boldsymbol{g}_2(\boldsymbol{x}_1(t), \boldsymbol{x}_2(t), \boldsymbol{\sigma}(t), t)$, $\boldsymbol{B}$ and $\Delta \boldsymbol{B}(\boldsymbol{\sigma}(t), t)$ are matrices of appropriate dimensions; $\boldsymbol{g}_1(\cdot)$, $\Delta \boldsymbol{g}_1(\cdot)$, $\boldsymbol{g}_2(\cdot)$, and $\Delta \boldsymbol{g}_2(\cdot)$ are continuous functions, which can be generalized to be Lebesgue measurable in t.

Remark 2. From Equation (32), the dynamic model of the VESS of the tank consisting of two subsystems is nonlinear, and its state variables $\boldsymbol{x}_1$ and $\boldsymbol{x}_2$ are coupled to each other, providing the dynamical model for the subsequent design of a robust backstepping controller.

Remark 3. There exists the matrix $\boldsymbol{L}(\boldsymbol{x}_1, \boldsymbol{x}_2)$ such that $\boldsymbol{P}^{\mathrm{T}} = \boldsymbol{B}\boldsymbol{L}$, that is, the input matrix satisfies the adjacency matched condition, and thus the input matrix $\boldsymbol{P}$ of subsystem N_1 can be described by the input matrix $\boldsymbol{B}$ of subsystem N_2. In other words, the control input $u(t)$ can make the dynamic link between the state variable $\boldsymbol{x}_1$ of subsystem N_1 and the state variable $\boldsymbol{x}_2$ of subsystem N_2, so that the control input $u(t)$ can realize the dynamic regulation of the whole system (including subsystems N_1 and N_2) although it enters the system from subsystem N_2.

Having established the formulation of the pitch-pointing tracking problem for the VESS, the next step is to design a robust control strategy that can effectively handle the system's flexible nonlinearity and mismatched uncertainty. In Section 5, we propose a robust backstepping control method that transforms the original mismatched uncertain system into a locally matched system. This transformation enables the design of a control law that ensures practical stability for both the original and reconfigured systems. The detailed design process, stability analysis, and simulation results are presented in the following section.

4 | Robust Backstepping Control Strategy for the VESS

Since the VESS considers flexible nonlinearity to be a mismatched uncertain system, the control method under

conventional logic is no longer applicable. The backstepping control idea is used to transform the state of the original controlled system, specifically from $\boldsymbol{x}$ to $\boldsymbol{z}$, so as to reconstruct the controlled system and make the reconstructed system satisfy the matched condition, and further design the robust controller to make the reconstructed system present practical stability while the original controlled system presents the same characteristics, so as to realize the barrel vertical stability control.

4.1 | Design of Robust Backstepping Controller

At first, choose the appropriate functions $\bar{g}_{12}(\cdot)$ and $\bar{g}_{22}(\cdot)$ to make the uncontrolled nominal systems $\boldsymbol{x}_1(t) = \boldsymbol{g}_1(\boldsymbol{x}_1(t), t)$ and $\boldsymbol{x}_2(t) = \boldsymbol{g}_2(\boldsymbol{x}_2(t), t)$ to be uniformly asymptotically stable at the origin $\boldsymbol{x} = 0$, then, choose the second-order differential functions $V_k(\cdot) : \mathbf{R}^2 \times \mathbf{R} \to \mathbf{R}_+, k = 1, 2$ and continuous, strictly increasing functions $\lambda_j^k(\cdot) : \mathbf{R}_+ \to \mathbf{R}_+, j = 1, 2$ are constructed to satisfy

$$\begin{aligned} \lambda_j^k(0) &= 0, \\ \lim_{r\to\infty} \lambda_j^k(r) &= \infty, \end{aligned} \tag{33}$$

besides, choose a strictly positive constant λ_3^k, such that for all $(\boldsymbol{x}_k, t) \in \mathbf{R}^2 \times \mathbf{R}$

$$\begin{aligned} &\lambda_1^k(\|\boldsymbol{x}_k\|) \le V_k(\boldsymbol{x}_k, t) \le \lambda_2^k(\|\boldsymbol{x}_k\|), \\ &\Gamma_0^k(\boldsymbol{x}_k, t) := \frac{\partial V_k(\boldsymbol{x}_k, t)}{\partial t} + \nabla_{\boldsymbol{x}_k}^{\mathrm{T}} V_k(\boldsymbol{x}_k, t) g_k(\boldsymbol{x}_k, t) \le -\lambda_3^k \|\boldsymbol{x}_k\|^2, \end{aligned} \tag{34}$$

In addition, exist a continuous function $\lambda_4^k(\cdot) : \mathbf{R}_+ \to \mathbf{R}_+, \lambda_4^k(0) = 0$, which satisfies

$$\left\| \frac{\partial V_k(\boldsymbol{x}_k, t)}{\partial \boldsymbol{x}_k} \right\| \le \lambda_4^k(\|\boldsymbol{x}_k\|), \tag{35}$$

which means that for the uncontrolled nominal systems $\boldsymbol{x}_1(t) = \boldsymbol{g}_1(\boldsymbol{x}_1(t), t)$ and $\boldsymbol{x}_2(t) = \boldsymbol{g}_2(\boldsymbol{x}_2(t), t)$, there exists the legal Lyapunov functions $V_1(\cdot)$ and $V_2(\cdot)$.

Then, the robust controller $\boldsymbol{v} = [v_1(t), v_2(t)]^{\mathrm{T}} \in \mathbf{R}^2$ is designed to induce the following system to present practical stability

$$\dot{\boldsymbol{x}}_1 = \boldsymbol{g}_1(\boldsymbol{x}_1(t), t) + \Delta \boldsymbol{g}_1(\boldsymbol{x}_1(t), \boldsymbol{\sigma}(t), t) + \boldsymbol{P}\boldsymbol{v}(t). \tag{36}$$

Considering that the system state variable $\boldsymbol{x}_2 = [F(t), \dot{F}(t)]$ and the matrix $\boldsymbol{P} = \begin{bmatrix} 0 & 0 \\ P_{21} & 0 \end{bmatrix}$, $v_2(t)$ can be described as

$$v_2(t) = \dot{v}_1(t) = \frac{\partial v_1}{\partial \boldsymbol{x}_1}\dot{\boldsymbol{x}}_1 + \frac{\partial v_1}{t}. \tag{37}$$

For discussing the boundary value of the uncertain term $\Delta \boldsymbol{g}_1$, according to Equation (31), Δg_{12} can be decomposed into the form of multiplying the "certain" and "uncertain" portions.

$$\begin{aligned} &\Delta g_{12}(x_{11}(t), x_{12}(t), \sigma_1(t), t) \\ &\quad = P_{21} q_{12}(x_{11}(t), x_{12}(t), \sigma_1(t), t), \end{aligned} \tag{38}$$

substituting it into Equation (32), we have

$$\begin{aligned} &\Delta \boldsymbol{g}_1(x_{11}(t), x_{12}(t), \sigma_1(t), t) \\ &= \begin{bmatrix} 0 \\ P_{21} q_{12}(x_{11}(t), x_{12}(t), \sigma_1(t), t) \end{bmatrix} \\ &= \begin{bmatrix} 0 & 0 \\ P_{21} & 0 \end{bmatrix} \begin{bmatrix} q_{12}(x_{11}(t), x_{12}(t), \sigma_1(t), t) \\ 0 \end{bmatrix} \\ &=: \boldsymbol{P}\boldsymbol{q}_1(x_{11}(t), x_{12}(t), \sigma_1(t), t) \\ &= \boldsymbol{P}\boldsymbol{q}_1(\boldsymbol{x}_1(t), \boldsymbol{\sigma}(t), t), \end{aligned} \tag{39}$$

where $\boldsymbol{q}_1(\cdot)$ is a continuous function of $\boldsymbol{x}_1(t), \boldsymbol{x}_2(t)$ and t.

In preparation for the subsequent controller design, the boundary conditions of $\boldsymbol{q}_1$ are now further analyzed

$$\begin{aligned} q_{12} &= P_{21}^{-1} \Delta g_{12} \\ &= P_{21}^{-1} \left[-\frac{1}{C_1} \Delta f_d + Z_1(x_{11}, x_{12}, t) - \bar{g}_{12} \right]. \end{aligned} \tag{40}$$

According $P_{21} = \frac{l_1}{C_1} > 0$, we have

$$\begin{aligned} \|\boldsymbol{q}_1\| = \|q_{12}\| &= P_{21}^{-1} \left| -\frac{1}{C_1} \Delta f_d + Z_1(x_{11}, x_{12}, t) - \bar{g}_{12} \right| \\ &\le P_{21}^{-1} \left(|Z_1(x_{11}, x_{12}, t)| + \frac{1}{C_1} |\Delta f_d| + |\bar{g}_{12}| \right) \\ &\le P_{21}^{-1} \left(|Z_1(x_{11}, x_{12}, t)| + \frac{1}{C_1} \hat{f}_d + |\bar{g}_{12}| \right) \\ &=: \eta_{\boldsymbol{q}_1}(\boldsymbol{x}_1, t), \end{aligned} \tag{41}$$

then, the controller is designed as $\boldsymbol{\mu}_1 = [\mu_{11}, \mu_{12}]^{\mathrm{T}} \in \mathbf{R}^2$, where

$$\begin{aligned} \mu_{11} &= \begin{cases} -\frac{\alpha}{\|\alpha\|} \eta_{\boldsymbol{q}_1}(\boldsymbol{x}_1, t) & \text{if } \|\alpha\| > \varepsilon_1, \\ -\sin\left(\frac{\pi\alpha}{2\varepsilon_1}\right) \eta_{\boldsymbol{q}_1}(\boldsymbol{x}_1, t) & \text{if } \|\alpha\| \le \varepsilon_1, \end{cases} \\ \mu_{12} &= v_2(t) = \frac{\partial v_1}{\partial \boldsymbol{x}_1}\dot{\boldsymbol{x}}_1 + \frac{\partial v_1}{t}, \end{aligned} \tag{42}$$

where

$$\alpha(\boldsymbol{x}_1, t) = \boldsymbol{P}_r^{\mathrm{T}} \nabla_{\boldsymbol{x}_1} V_1(\boldsymbol{x}_1, t) \eta_{\boldsymbol{q}_1}(\boldsymbol{x}_1, t), \tag{43}$$

where $\boldsymbol{P}_r = [0, P_{21}]^{\mathrm{T}}, \varepsilon_1 > 0$ is the design parameter and $\mu_{11}(\cdot)$ is a continuous differentiable smooth function and $\|\boldsymbol{\mu}_2\| \le \|\mu_{11}\| \le \eta_{\boldsymbol{q}_1}$.

Theorem 1. *When the controller (42) is applied to the controlled system (36), the solution of this controlled system will exhibit practical stability as follows:*

I. *Uniform boundedness: For any* $\rho > 0$, *there exists a positive real number* $\chi(\rho) \leq \infty$ *such that if* $\|\boldsymbol{x}_1(t_0)\| < \rho$, *then* $\|\boldsymbol{x}_1(t)\| \leqslant \chi(\rho)$ *for all* $t \geqslant t_0$;

II. *Uniform ultimate boundedness: For any* $\rho > 0$ *and* $\bar{\chi} > \underline{\chi}$, *there exists* $\underline{\chi} > 0$ *such that if* $\|\boldsymbol{x}_1(t_0)\| < \rho$, *then* $\|\boldsymbol{x}_1(t)\| \leqslant \bar{\chi}$ *for all* $t \geqslant T(\bar{\chi}, \rho)$, *where* $T(\bar{\chi}, \rho) < \infty$;

III. *Uniform stability: There exists a real number* $\phi(\bar{\chi}) > 0$ *such that if* $\|\boldsymbol{x}_1(t_0)\| \leqslant \phi(\bar{\chi})$, *then* $\|\boldsymbol{x}(t)\| \leqslant \bar{\chi}$ *for* $t \geqslant t_0$.

Proof. With control $\mu_1(\cdot)$, the derivative function of the Lyapunov function $V_1(\cdot)$ along the trajectory of the system (36) is

$$\Gamma_1 := \Gamma_0^1 + \nabla_{\boldsymbol{x}_1}^{\mathrm{T}} V_1(\Delta \boldsymbol{g}_1(\boldsymbol{x}_1(t), \boldsymbol{\sigma}(t), t) + \boldsymbol{P}\boldsymbol{\mu}_1). \tag{44}$$

Recalling $\Delta \boldsymbol{g}_1 = \boldsymbol{P}\boldsymbol{q}_1$ and with Equation (34)

$$\begin{aligned} \Gamma_1 &\leqslant -\lambda_3^1 \|\boldsymbol{x}_1\|^2 + \nabla_{\boldsymbol{x}_1}^{\mathrm{T}} V_1(\boldsymbol{P}\boldsymbol{q}_1 + \boldsymbol{P}\boldsymbol{\mu}_1) \\ &= -\lambda_3^1 \|\boldsymbol{x}_1\|^2 + \nabla_{\boldsymbol{x}_1}^{\mathrm{T}} V_1 \boldsymbol{P}_r q_{12} + \nabla_{\boldsymbol{x}_1}^{\mathrm{T}} V_1 \boldsymbol{P}_r \mu_{11}. \end{aligned} \tag{45}$$

Let $\Psi_1 = \boldsymbol{P}_r{}^{\mathrm{T}} \nabla_{\boldsymbol{x}_1} V_1$, according to Equation (42), if $\|\alpha\| > \varepsilon_1$

$$\begin{aligned} \Gamma_1 &\leqslant -\lambda_3^1 \|\boldsymbol{x}_1\|^2 + \|\Psi_1\| \eta_{\boldsymbol{q}_1} - \Psi_1^{\mathrm{T}} \frac{\Psi_1 \eta_{\boldsymbol{q}_1}}{\|\Psi_1 \eta_{\boldsymbol{q}_1}\|} \eta_{\boldsymbol{q}_1} \\ &= -\lambda_3^1 \|\boldsymbol{x}_1\|^2. \end{aligned} \tag{46}$$

if $\|\alpha\| \leqslant \varepsilon_1$

$$\begin{aligned} \Gamma_1 &\leqslant -\lambda_3^1 \|\boldsymbol{x}_1\|^2 + \nabla_{\boldsymbol{x}_1}^{\mathrm{T}} V_1 \boldsymbol{P}_r q_{12} + \nabla_{\boldsymbol{x}_1}^{\mathrm{T}} V_1 \boldsymbol{P}_r \mu_{11} \\ &\leqslant -\lambda_3^1 \|\boldsymbol{x}_1\|^2 + \left\| \nabla_{\boldsymbol{x}_1}^{\mathrm{T}} V_1 \boldsymbol{P}_r \right\| \eta_{\boldsymbol{q}_1} \\ &\quad - \nabla_{\boldsymbol{x}_1}^{\mathrm{T}} V_1 \boldsymbol{P}_r \sin\left(\frac{\pi \boldsymbol{P}_r{}^{\mathrm{T}} \nabla_{\boldsymbol{x}_1} V_1 \eta_{\boldsymbol{q}_1}}{2\varepsilon_1} \right) \eta_{\boldsymbol{q}_1} \\ &\leqslant -\lambda_3^1 \|\boldsymbol{x}_1\|^2 + \|\alpha\| + \|\alpha\| \\ &\leqslant -\lambda_3^1 \|\boldsymbol{x}_1\|^2 + 2\varepsilon_1. \end{aligned} \tag{47}$$

Consequently, for all $(\boldsymbol{x}_1, t)$

$$\Gamma_1 \leqslant -\lambda_3^1 \|\boldsymbol{x}_1\|^2 + 2\varepsilon_1. \tag{48}$$

This means that the controlled system (36) exhibits practical stability under the action of control (42).

Since subsystem N_1(32) actually contains $\boldsymbol{x}_2$ rather than control $\boldsymbol{\mu}_1$, defining the implanted control

$$\boldsymbol{v}(t) = \boldsymbol{\mu}_1(\boldsymbol{x}_1(t), t) - \gamma_1 \boldsymbol{P}^{\mathrm{T}} \nabla_{\boldsymbol{x}_1} V_1(\boldsymbol{x}_1, t), \tag{49}$$

where γ_1 is the scalar design parameter and the new term $\gamma_1 \boldsymbol{P}^{\mathrm{T}} \nabla_{\boldsymbol{x}_1} V_1$ is added to compensate for the difference between $\boldsymbol{x}_2$ and $\boldsymbol{v}$. Substituting $\boldsymbol{x}_2 = \boldsymbol{v} + \boldsymbol{x}_2 - \boldsymbol{v}$ into Equation (32), the subsystem N_1 can be redescribed as

$$\begin{aligned} (N_1)\dot{\boldsymbol{x}}_1(t) = \boldsymbol{g}_1(\boldsymbol{x}_1(t), t) + \Delta \boldsymbol{g}_1(\boldsymbol{x}_1(t), \boldsymbol{\sigma}(t), t) + \boldsymbol{P}\boldsymbol{v}(t) \\ + \boldsymbol{P}(\boldsymbol{x}_2(t) - \boldsymbol{v}(t)). \end{aligned} \tag{50}$$

Recalling $\boldsymbol{P}_r = [0, P_{21}]^{\mathrm{T}}$ and Equation (49), $v_1(t)$ can be described as

$$v_1(t) = \mu_{11}(\boldsymbol{x}_1(t), t) - \gamma_1 \boldsymbol{P}_r{}^{\mathrm{T}} \nabla_{\boldsymbol{x}_1} V_1(\boldsymbol{x}_1, t). \tag{51}$$

Based on control $\boldsymbol{v}$, the derivative function of $V_1(\cdot)$ is

$$\begin{aligned} \Gamma_1 &:= \Gamma_0^1 + \nabla_{\boldsymbol{x}_1}^{\mathrm{T}} V_1(\Delta \boldsymbol{g}_1 + \boldsymbol{P}\boldsymbol{v} + \boldsymbol{P}(\boldsymbol{x}_2 - \boldsymbol{v})) \\ &= \Gamma_0^1 + \nabla_{\boldsymbol{x}_1}^{\mathrm{T}} V_1 \left[\Delta \boldsymbol{g}_1 + \boldsymbol{P}\left(\boldsymbol{\mu}_1 - \gamma_1 \boldsymbol{P}^{\mathrm{T}} \nabla_{\boldsymbol{x}_1} V_1 \right) + \boldsymbol{P}(\boldsymbol{x}_2 - \boldsymbol{v}) \right] \\ &= \Gamma_0^1 + \nabla_{\boldsymbol{x}_1}^{\mathrm{T}} V_1(\Delta \boldsymbol{g}_1 + \boldsymbol{P}\boldsymbol{\mu}_1) \\ &\quad - \nabla_{\boldsymbol{x}_1}^{\mathrm{T}} V_1 \boldsymbol{P}\gamma_1 \boldsymbol{P}^{\mathrm{T}} \nabla_{\boldsymbol{x}_1} V_1 + \nabla_{\boldsymbol{x}_1}^{\mathrm{T}} V \boldsymbol{P}(\boldsymbol{x}_2 - \boldsymbol{v}). \end{aligned} \tag{52}$$

With $\|\boldsymbol{P}^{\mathrm{T}} \nabla_{\boldsymbol{x}_1} V_1\| = \|\boldsymbol{P}_r{}^{\mathrm{T}} \nabla_{\boldsymbol{x}_1} V\| = \|\Psi_1\|$ and Equation (48), we have

$$\Gamma_1 \leqslant -\lambda_3^1 \|\boldsymbol{x}_1\|^2 + 2\varepsilon_1 - \gamma_1 \|\Psi_1\|^2 + \|\Psi_1\| \, \|\boldsymbol{x}_2 - \boldsymbol{v}\|. \tag{53}$$

The analysis of the third and fourth terms on the right-hand side of the inequality will be given later.

Then, the system state variable $\boldsymbol{x}_2$ is converted to $\boldsymbol{z}_2 = [z_{21}, z_{22}]^{\mathrm{T}} (\boldsymbol{z}_2 := \boldsymbol{x}_2 - \boldsymbol{v})$. According to Equation (32)

$$\begin{aligned} \dot{\boldsymbol{z}}_2 &= \dot{\boldsymbol{x}}_2 - \dot{\boldsymbol{v}} \\ &= \boldsymbol{g}_2(\boldsymbol{x}_2(t), t) + \Delta \boldsymbol{g}_2(\boldsymbol{x}_1(t), \boldsymbol{x}_2(t), \boldsymbol{\sigma}(t), t) \\ &\quad + (\boldsymbol{B} + \Delta \boldsymbol{B}(\boldsymbol{\sigma}(t), t))u(t) - \left[\frac{\partial \boldsymbol{v}}{\partial \boldsymbol{x}_1} \dot{\boldsymbol{x}}_1 + \frac{\partial \boldsymbol{v}}{\partial t} \right], \end{aligned} \tag{54}$$

according to Equation (32), defining

$$\begin{aligned} \frac{\partial \boldsymbol{v}}{\partial \boldsymbol{x}_1} \dot{\boldsymbol{x}}_1 + \frac{\partial \boldsymbol{v}}{\partial t} &= \frac{\partial \boldsymbol{v}}{\partial \boldsymbol{x}_1} (\boldsymbol{g}_1(\boldsymbol{x}_1, t) + \Delta \boldsymbol{g}_1(\boldsymbol{x}_1, \boldsymbol{\sigma}, t) + \boldsymbol{P}\boldsymbol{x}_2) + \frac{\partial \boldsymbol{v}}{\partial t} \\ &=: \boldsymbol{\Pi}_1(\boldsymbol{x}_1, \boldsymbol{x}_2, \boldsymbol{\sigma}, t). \end{aligned} \tag{55}$$

By introducing function $\boldsymbol{g}_2(\boldsymbol{z}_2, t) = \begin{bmatrix} z_{22}(t) \\ \bar{g}_{22}(z_{21}(t), z_{22}(t), t) \end{bmatrix}$, Equation (54) can be rewritten as

$$\begin{aligned} \dot{\boldsymbol{z}}_2 &= \boldsymbol{g}_2(\boldsymbol{z}_2, t) - \boldsymbol{g}_2(\boldsymbol{z}_2, t) + \boldsymbol{g}_2(\boldsymbol{x}_2, t) + \Delta \boldsymbol{g}_2(\boldsymbol{x}_1, \boldsymbol{x}_2, \boldsymbol{\sigma}, t) \\ &\quad + (\boldsymbol{B} + \Delta \boldsymbol{B}(\boldsymbol{\sigma}, t))u(t) - \boldsymbol{\Pi}_1(\boldsymbol{x}_1, \boldsymbol{x}_2, \boldsymbol{\sigma}, t) \\ &= \boldsymbol{g}_2(\boldsymbol{z}_2, t) + \Delta \boldsymbol{g}_2(\boldsymbol{x}_1, \boldsymbol{x}_2, \boldsymbol{\sigma}, t) + \boldsymbol{g}_2(\boldsymbol{x}_2, t) - \boldsymbol{g}_2(\boldsymbol{z}_2, t) \\ &\quad - \boldsymbol{\Pi}_1(\boldsymbol{x}_1, \boldsymbol{x}_2, \boldsymbol{\sigma}, t) + (\boldsymbol{B} + \Delta \boldsymbol{B}(\boldsymbol{\sigma}, t))u(t) \\ &= \boldsymbol{g}_2(\boldsymbol{z}_2, t) + \Delta \boldsymbol{a}_2(\boldsymbol{x}_1, \boldsymbol{x}_2, \boldsymbol{\sigma}, \boldsymbol{z}_2, t) \\ &\quad + (\boldsymbol{B} + \Delta \boldsymbol{B}(\boldsymbol{\sigma}, t))u(t), \end{aligned} \tag{56}$$

where

$$\begin{aligned} \Delta \boldsymbol{a}_2(\boldsymbol{x}_1, \boldsymbol{x}_2, \boldsymbol{\sigma}, \boldsymbol{z}_2, t) = \; & \Delta \boldsymbol{g}_2(\boldsymbol{x}_1, \boldsymbol{x}_2, \boldsymbol{\sigma}, t) + \boldsymbol{g}_2(\boldsymbol{x}_2, t) \\ & - \boldsymbol{g}_2(\boldsymbol{z}_2, t) - \boldsymbol{\Pi}_1(\boldsymbol{x}_1, \boldsymbol{x}_2, \boldsymbol{\sigma}, t). \end{aligned} \tag{57}$$

With Equations (31), (32), (55) and the definitions of $\boldsymbol{z}_2$ and $\boldsymbol{g}_2(\boldsymbol{z}_2, t)$, Equation (57) can be rewritten as

$$
\begin{aligned}
&\Delta \boldsymbol{a}_2(\boldsymbol{x}_1, \boldsymbol{x}_2, \boldsymbol{\sigma}, \boldsymbol{z}_2, \boldsymbol{t}) \\
&= \begin{bmatrix} 0 \\ \Delta g_{22}(x_{11}(t), x_{12}(t), x_{21}(t), x_{22}(t), \sigma_1(t), \sigma_2(t), t) \end{bmatrix} \\
&\quad + \begin{bmatrix} x_{22}(t) \\ \bar{g}_{22}(x_{21}(t), x_{22}(t), t) \end{bmatrix} - \begin{bmatrix} z_{22}(t) \\ \bar{g}_{22}(z_{21}(t), z_{22}(t), t) \end{bmatrix} \\
&\quad - \begin{bmatrix} v_2(t) \\ \dfrac{\partial v_2}{\partial \boldsymbol{x}_1}(\boldsymbol{g}_1(\boldsymbol{x}_1, t) + \Delta \boldsymbol{g}_1(\boldsymbol{x}_1, \boldsymbol{\sigma}, t) + \boldsymbol{P}\boldsymbol{x}_2) + \dfrac{\partial v_2}{\partial t} \end{bmatrix} \\
&= \begin{bmatrix} 0 \\ \Delta a_{22}(x_{11}(t), x_{12}(t), x_{21}(t), x_{22}(t), z_{21}(t), z_{22}(t) \\ , \sigma_1(t), \sigma_2(t), t) \end{bmatrix},
\end{aligned} \tag{58}
$$

where

$$
\begin{aligned}
\Delta a_{22} &= \Delta k_{se} S(x_{11}, x_{12}, x_{21}, t) \\
&\quad + \frac{l_1 l_3 K_a K_b}{C_1}(\Delta k_{se} \bar{f}_d + \bar{k}_{se} \Delta f_d + \Delta k_{se} \Delta f_d) + Z_2(x_{11}, x_{12}, x_{21}, t) \\
&\quad + g_{22}(x_{12}, x_{12}, x_{21}, x_{22}, t) - \bar{g}_{22}(x_{21}, x_{22}, t) \\
&\quad + \bar{g}_{22}(x_{21}, x_{22}, t) - \bar{g}_{22}(z_{21}, z_{22}, t) \\
&\quad - \frac{\partial v_2}{\partial \boldsymbol{x}_1}(\boldsymbol{g}_1(\boldsymbol{x}_1, t) + \Delta \boldsymbol{g}_1(\boldsymbol{x}_1, \boldsymbol{\sigma}, t) + \boldsymbol{P}\boldsymbol{x}_2) - \frac{\partial v_2}{\partial t} \\
&= \Delta k_{se} S(x_{11}, x_{12}, x_{21}, t) \\
&\quad + \frac{l_1 l_3 K_a K_b}{C_1}(\Delta k_{se} \bar{f}_d + \bar{k}_{se} \Delta f_d + \Delta k_{se} \Delta f_d) + Z_2(x_{11}, x_{12}, x_{21}, t) \\
&\quad + g_{22}(x_{12}, x_{12}, x_{21}, x_{22}, t) - \bar{g}_{22}(z_{21}, z_{22}, t) \\
&\quad - \frac{\partial v_2}{\partial \boldsymbol{x}_1}(\boldsymbol{g}_1(\boldsymbol{x}_1, t) + \boldsymbol{P}\boldsymbol{q}_1(\boldsymbol{x}_1(t), \boldsymbol{\sigma}(t), t) + \boldsymbol{P}\boldsymbol{x}_2) + \frac{\partial v_2}{\partial t}.
\end{aligned} \tag{59}
$$

Considering that Δa_{22}, B_{21}, ΔB_{21} are continuous functions and B_{21} is a positive scalar, Δa_{22} and ΔB_{21} can be decomposed into the form of multiplying the "certain" and "uncertain" portions:

$$
\begin{aligned}
&\Delta a_{22}(x_{11}(t), x_{12}(t), x_{21}(t), x_{22}(t), z_{21}(t), z_{22}(t), \sigma_1(t), \sigma_2(t), t) \\
&= B_{21} q_{21}(x_{11}(t), x_{12}(t), x_{21}(t), x_{22}(t), z_{21}(t), z_{22}(t), \sigma_1(t), \sigma_2(t), t).
\end{aligned} \tag{60}
$$

$$
\Delta B_{21}(\sigma_1, t) = B_{21} E_{21}(\sigma_1, t). \tag{61}
$$

Substituting it into Equation (32), we have

$$
\begin{aligned}
&\Delta \boldsymbol{a}_2(\boldsymbol{x}_1, \boldsymbol{x}_2, \boldsymbol{\sigma}, \boldsymbol{z}_2, t) \\
&= \boldsymbol{B} q_{21}(x_{11}(t), x_{12}(t), x_{21}(t), x_{22}(t), z_{21}(t), z_{22}(t), \sigma_1(t), \sigma_2(t), t) \\
&= \boldsymbol{B}\boldsymbol{q}_2(\boldsymbol{x}_1, \boldsymbol{x}_2, \boldsymbol{\sigma}, \boldsymbol{z}_2, t).
\end{aligned} \tag{62}
$$

$$
\Delta \boldsymbol{B}(\boldsymbol{\sigma}, t) = \boldsymbol{B} E_{21}(\sigma_1, t) = \boldsymbol{B}\boldsymbol{E}_2(\boldsymbol{\sigma}, t). \tag{63}
$$

In preparation for the subsequent controller design, the boundary conditions $\boldsymbol{q}_2$ and $\boldsymbol{E}_2$ are now further analyzed, according to Equations (31) and (59), we have

$$
\begin{aligned}
\boldsymbol{q}_2 &= B_{21}^{-1} \Delta a_{22} \\
&= B_{21}^{-1}\Big[\frac{\partial v_2}{\partial t}\Delta k_{se} S(x_{11}, x_{12}, x_{21}, t) \\
&\quad + \frac{l_1 l_3 K_a K_b}{C_1}(\Delta k_{se} \bar{f}_d + \bar{k}_{se} \Delta f_d + \Delta k_{se} \Delta f_d) + Z_2(x_{11}, x_{12}, x_{21}, t) \\
&\quad + g_{22}(x_{12}, x_{12}, x_{21}, x_{22}, t) - \bar{g}_{22}(z_{21}, z_{22}, t) \\
&\quad - \frac{\partial v_2}{\partial \boldsymbol{x}_1}(\boldsymbol{g}_1(\boldsymbol{x}_1, t) + \Delta \boldsymbol{g}_1(\boldsymbol{x}_1, \boldsymbol{\sigma}, t) + \boldsymbol{P}\boldsymbol{x}_2) + \frac{\partial v_2}{\partial t}\Big],
\end{aligned} \tag{64}
$$

$$
\boldsymbol{E}_2 = B_{21}^{-1} \Delta B_{21} = \frac{\Delta k_{se}}{\bar{k}_{se}}, \tag{65}
$$

where the uncertain portion of axial stiffness of the electric cylinder Δk_{se} usually fluctuates in the range of 10%–20% of the certain portion of axial stiffness of the electric cylinder k_{se}, so existing constant $\eta_{E_2} > -1$ to make $E_2 \geqslant \eta_{E_2} > -1$. For obtaining $\|q_2\|$, the following projection is made

$$
\begin{aligned}
\|\boldsymbol{q}_2\| &= B_{21}^{-1}\Big[\frac{\partial v_2}{\partial t}\Delta k_{se} S(x_{11}, x_{12}, x_{21}, t) \\
&\quad + \frac{l_1 l_3 K_a K_b}{C_1}(\Delta k_{se} \bar{f}_d + \bar{k}_{se} \Delta f_d + \Delta k_{se} \Delta f_d) + Z_2(x_{11}, x_{12}, x_{21}, t) \\
&\quad + g_{22}(x_{12}, x_{12}, x_{21}, x_{22}, t) - \bar{g}_{22}(z_{21}, z_{22}, t) \\
&\quad - \frac{\partial v_2}{\partial \boldsymbol{x}_1}(\boldsymbol{g}_1(\boldsymbol{x}_1, t) + \boldsymbol{P}\boldsymbol{q}_1(\boldsymbol{x}_1(t), \boldsymbol{\sigma}(t), t) + \boldsymbol{P}\boldsymbol{x}_2) + \frac{\partial v_2}{\partial t}\Big] \\
&\leqslant \Big|B_{21}^{-1}\Big|\Big[\hat{k}_{se}|S(\boldsymbol{x}_1, \boldsymbol{x}_2, t)| + \Big|\frac{l_1 l_3 K_a K_b}{C_1}\Big|(\hat{k}_{se}|\hat{\bar{f}}_d| + |\hat{\bar{k}}_{se}|\hat{f}_d + \hat{k}_{se}\hat{f}_d) \\
&\quad + |Z_2(\boldsymbol{x}_1, \boldsymbol{x}_2, t) + g_{22}(\boldsymbol{x}_1, \boldsymbol{x}_2, t) - \bar{g}_{22}(z_{21}, z_{22}, t)| + \Big|\frac{\partial v_2}{\partial \boldsymbol{x}_1}\boldsymbol{P}\Big| \eta_{\boldsymbol{q}_1} \\
&\quad + \Big|\frac{\partial v_2}{\partial \boldsymbol{x}_1}(\boldsymbol{g}_1(\boldsymbol{x}_1, t) + \boldsymbol{P}\boldsymbol{x}_2) + \frac{\partial v_2}{\partial t}\Big|\Big| =: \eta_{\boldsymbol{q}_2}(\boldsymbol{x}_1, \boldsymbol{x}_2, \boldsymbol{z}_2, t).
\end{aligned} \tag{66}
$$

Finally, to achieve stability tracking control of the VESS with flexible nonlinearity, the following robust backstepping controller is designed for the controlled system:

$$
u(t) = \mu_2(\boldsymbol{x}_1, \boldsymbol{x}_2, \boldsymbol{z}_2, t), \tag{67}
$$

where

$$
\mu_2 = \begin{cases} -\dfrac{\beta}{\|\beta\|}\eta_2(\boldsymbol{x}_1, \boldsymbol{x}_2, \boldsymbol{z}_2, t) & \text{if } \|\beta\| > \varepsilon_2, \\ -\dfrac{\beta}{\varepsilon_2}\eta_2(\boldsymbol{x}_1, \boldsymbol{x}_2, \boldsymbol{z}_2, t) & \text{if } \|\beta\| \leqslant \varepsilon_2, \end{cases} \tag{68}
$$

$$
\eta_2(\boldsymbol{x}_1, \boldsymbol{x}_2, \boldsymbol{z}_2, t) = \frac{\eta_{\boldsymbol{q}_2}(\boldsymbol{x}_1, \boldsymbol{x}_2, \boldsymbol{z}_2, t)}{1 + \eta_{E_2}}, \tag{69}
$$

$$
\beta(\boldsymbol{x}_1, \boldsymbol{x}_2, \boldsymbol{z}_2, t) = \boldsymbol{B}^{\mathrm{T}} \nabla_{\boldsymbol{z}_2} V_2(\boldsymbol{z}_2, t) \eta_2(\boldsymbol{x}_1, \boldsymbol{x}_2, \boldsymbol{z}_2, t), \tag{70}
$$

where $\varepsilon_2 > 0$ is the design parameter, $\eta_{E_2} > -1$, $\eta_{\mathbf{q}_2} > 0$, thus $\eta_2 > 0$. Similar to the analysis of α, β can be ensured to be non-zero by picking the appropriate function V_2. With control $u(t)$, the derivative function of the Lyapunov function $V_2(\cdot)$ along the trajectory of the system (56) is

$$\Gamma_2 := \Gamma_0^2 + \nabla_{z_2}^{\mathrm{T}} V_2(\Delta \boldsymbol{a}_2(\boldsymbol{x}_1, \boldsymbol{x}_2, \boldsymbol{\sigma}, \boldsymbol{z}_2, t) + (\boldsymbol{B} + \Delta \boldsymbol{B}(\boldsymbol{\sigma}, t))u(t)). \tag{71}$$

Recalling $\Delta \boldsymbol{a}_2 = \boldsymbol{B}\boldsymbol{q}_2$ and $\Delta \boldsymbol{B} = \boldsymbol{B}\boldsymbol{E}_2$, according to Equation (34), we have

$$\begin{aligned}\Gamma_2 \leqslant & -\lambda_3^2 \|\boldsymbol{z}_2\|^2 + \nabla_{z_2}^{\mathrm{T}} V_2(\boldsymbol{B}\boldsymbol{q}_2(\boldsymbol{x}_1, \boldsymbol{x}_2, \boldsymbol{\sigma}, \boldsymbol{z}_2, t) \\ & + \boldsymbol{B}u(t) + \boldsymbol{B}\boldsymbol{E}_2(\boldsymbol{\sigma}, t)u(t)) \\ = & -\lambda_3^2 \|\boldsymbol{z}_2\|^2 + \nabla_{z_2}^{\mathrm{T}} V_2 \boldsymbol{B}\boldsymbol{q}_2(\boldsymbol{x}_1, \boldsymbol{x}_2, \boldsymbol{\sigma}, \boldsymbol{z}_2, t) \\ & + \nabla_{z_2}^{\mathrm{T}} V_2 \boldsymbol{B}u(t) + \nabla_{z_2}^{\mathrm{T}} V_2 \boldsymbol{B}\boldsymbol{E}_2(\boldsymbol{\sigma}, t)u(t).\end{aligned} \tag{72}$$

According to Equation (67), if $\|\beta\| > \varepsilon_2$

$$\begin{aligned}\Gamma_2 \leqslant & -\lambda_3^2 \|\boldsymbol{z}_2\|^2 + \nabla_{z_2}^{\mathrm{T}} V_2 \boldsymbol{B}\boldsymbol{q}_2(\boldsymbol{x}_1, \boldsymbol{x}_2, \boldsymbol{\sigma}, \boldsymbol{z}_2, t) \\ & - \nabla_{z_2}^{\mathrm{T}} V_2 \boldsymbol{B} \frac{\boldsymbol{B}^{\mathrm{T}} \nabla_{z_2} V_2 \eta_2}{\|\boldsymbol{B}^{\mathrm{T}} \nabla_{z_2} V_2 \eta_2\|} \eta_2 \\ & - \nabla_{z_2}^{\mathrm{T}} V_2 \boldsymbol{B}\boldsymbol{E}_2 \frac{\boldsymbol{B}^{\mathrm{T}} \nabla_{z_2} V_2 \eta_2}{\|\boldsymbol{B}^{\mathrm{T}} \nabla_{z_2} V_2 \eta_2\|} \eta_2.\end{aligned} \tag{73}$$

Let $\psi_2 = \boldsymbol{B}^{\mathrm{T}} \nabla_{z_2} V_2$, Equation (73) can be rewritten as

$$\begin{aligned}\Gamma_2 = & -\lambda_3^2 \|\boldsymbol{z}_2\|^2 + \Psi_2^{\mathrm{T}} \boldsymbol{q}_2(\boldsymbol{x}_1, \boldsymbol{x}_2, \boldsymbol{\sigma}, \boldsymbol{z}_2, t) \\ & - \Psi_2^{\mathrm{T}} \frac{\Psi_2 \eta_2}{\|\Psi_2\|} - \Psi_2^{\mathrm{T}} \boldsymbol{E}_2 \frac{\Psi_2 \eta_2}{\|\Psi_2\|}.\end{aligned} \tag{74}$$

Recalling $\|\boldsymbol{q}_2\| \leqslant \eta_{\boldsymbol{q}_2}$, $E_2 \geqslant \eta_{E_2} > -1$, $\eta_{\boldsymbol{q}_2} = (1 + \eta_{E_2})\eta_2$, we have

$$\begin{aligned}\Gamma_2 \leqslant & -\lambda_3^2 \|\boldsymbol{z}_2\|^2 + \|\Psi\| \eta_{\boldsymbol{q}_2} - \|\Psi\| \eta_2 - \|\Psi\| \eta_{E_2} \eta_2 \\ = & -\lambda_3^2 \|\boldsymbol{z}_2\|^2.\end{aligned} \tag{75}$$

According to Equation (67), if $\|\beta\| \leqslant \varepsilon_2$

$$\begin{aligned}\Gamma_2 \leqslant & -\lambda_3^2 \|\boldsymbol{z}_2\|^2 + \nabla_{z_2}^{\mathrm{T}} V_2 \boldsymbol{B}\boldsymbol{q}_2(\boldsymbol{x}_1, \boldsymbol{x}_2, \boldsymbol{\sigma}, \boldsymbol{z}_2, t) \\ & - \nabla_{z_2}^{\mathrm{T}} V_2 \boldsymbol{B} \frac{\boldsymbol{B}^{\mathrm{T}} \nabla_{z_2} V_2 \eta_2}{\varepsilon_2} \eta_2 - \nabla_{z_2}^{\mathrm{T}} V_2 \boldsymbol{B}\boldsymbol{E}_2 \frac{\boldsymbol{B}^{\mathrm{T}} \nabla_{z_2} V_2 \eta_2}{\varepsilon_2} \eta_2 \\ \leqslant & -\lambda_3^2 \|\boldsymbol{z}_2\|^2 + \|\beta\| \left(1 + \eta_{E_2}\right) - \frac{\|\beta\|^2}{\varepsilon_2} - \frac{\eta_{E_2} \|\beta\|^2}{\varepsilon_2} \\ \leqslant & -\lambda_3^2 \|\boldsymbol{z}_2\|^2 + \frac{\varepsilon_2 (1 + \eta_{E_2})}{4}.\end{aligned} \tag{76}$$

Consequently, for all $(\boldsymbol{z}_2, t)$

$$\Gamma_2 \leqslant -\lambda_3^2 \|\boldsymbol{z}_2\|^2 + \frac{\varepsilon_2 (1 + \eta_{E_2})}{4}. \tag{77}$$

□

4.2 | Stability Analysis of the Reconfigured System

For efficiently designing the robust backstepping controller, the state variables of the controlled system (32) are transformed and the transformation process can be summarized as

$$\begin{aligned}\boldsymbol{z}_1 &= \boldsymbol{x}_1, \\ \boldsymbol{z}_2 &= \boldsymbol{x}_2 - \boldsymbol{\nu},\end{aligned} \tag{78}$$

where $\boldsymbol{x} = [\boldsymbol{x}_1, \boldsymbol{x}_2]^{\mathrm{T}}$ is the pre-transformation state variables, $\boldsymbol{z} = [\boldsymbol{z}_1, \boldsymbol{z}_2]^{\mathrm{T}}$ is the post-transformation state variables, $\boldsymbol{\nu}$ is the implanted controller. The dynamics of the transformed state variables $\boldsymbol{z}$, that is, the reconfigured system dynamics can be described as

$$\begin{aligned}(\hat{N}_1)\dot{\boldsymbol{z}}_1(t) = & \boldsymbol{g}_1(\boldsymbol{z}_1(t), t) + \Delta \boldsymbol{g}_1(\boldsymbol{z}_1(t), \boldsymbol{\sigma}(t), t) + \boldsymbol{P}(\boldsymbol{z}_2(t) \\ & + \boldsymbol{\nu}(t)), \\ (\hat{N}_2)\dot{\boldsymbol{z}}_2(t) = & \boldsymbol{g}_2(\boldsymbol{z}_2(t) + \boldsymbol{\nu}(t), t) + \Delta \boldsymbol{g}_2(\boldsymbol{z}_1(t), \boldsymbol{z}_2(t) \\ & + \boldsymbol{\nu}(t), \boldsymbol{\sigma}(t), t) + (\boldsymbol{B} + \Delta \boldsymbol{B}(\boldsymbol{\sigma}(t), t))u(t) - \dot{\boldsymbol{\nu}}(t).\end{aligned} \tag{79}$$

Remark 4. To deal with the mismatched uncertainty disturbance in the VESS, the original controlled system (32) is reconstructed based on the system state transformation, so that the reconstructed system (79) meets the matched condition, and thus a robust backstepping controller is designed. If the controller can make the reconstructed system (79) and the original VESS (32) present practical stability, the tank pitch-pointing tracking control can be realized.

Theorem 2. *When the controller (67) is applied to the controlled system (79), the solution of this controlled system will exhibit practical stability as follows:*

I. *Uniform boundedness: For any $\rho_z > 0$, there exists a positive real number $\chi_z(\rho_z) \leqslant \infty$ such that if $\|\boldsymbol{z}(t_0)\| \leqslant \rho_z$, then $\|\boldsymbol{z}(t)\| \leqslant \chi_z(\rho_z)$ for all $t \geqslant t_0$.*

II. *Uniform ultimate boundedness: For any $\rho_z > 0$ and $\bar{\chi}_z > \underline{\chi}_z$, there exists $\underline{\chi}_z > 0$ such that if $\|\boldsymbol{z}(t_0)\| \leqslant \rho_z$, then $\|\boldsymbol{z}(t)\| \leqslant \bar{\chi}_z$ for all $t \geqslant T_z(\bar{\chi}_z, \rho_z)$, where $T_z(\bar{\chi}_z, \rho_z) < \infty$.*

III. *Uniform stability: There exists a real number $\phi_z(\bar{\chi}_z) > 0$ such that if $\|\boldsymbol{z}(t_0)\| \leqslant \phi_z(\bar{\chi}_z)$, then $\|\boldsymbol{z}(t)\| \leqslant \bar{\chi}_z$ for $t \geqslant t_0$.*

Proof. Choosing the Lyapunov function candidate

$$V(\boldsymbol{z}, t) = V_1(\boldsymbol{z}_1, t) + V_2(\boldsymbol{z}_2, t). \tag{80}$$

The derivative function of the Lyapunov function $V(\cdot)$ along the trajectory of the system (79) is

$$\Gamma(\boldsymbol{z}, t) = \Gamma_1(\boldsymbol{z}_1, t) + \Gamma_2(\boldsymbol{z}_2, t). \tag{81}$$

With Equations (53) and (77), we have

$$\begin{aligned}\Gamma(\boldsymbol{z}, t) \leqslant & -\lambda_3^1 \|\boldsymbol{z}_1\|^2 + 2\varepsilon_1 - \gamma_1 \|\psi_1\|^2 + \|\psi_1\| \|\boldsymbol{z}_2\| \\ & - \lambda_3^2 \|\boldsymbol{z}_2\|^2 + \frac{\varepsilon_2 (1 + \eta_{E_2})}{4} \\ = & -\lambda_3^1 \|\boldsymbol{z}_1\|^2 - \gamma_1 \|\psi_1\|^2 + \|\psi_1\| \|\boldsymbol{z}_2\| \\ & - \lambda_3^2 \|\boldsymbol{z}_2\|^2 + 2\varepsilon_1 + \frac{\varepsilon_2 (1 + \eta_{E_2})}{4}.\end{aligned} \tag{82}$$

Then, Using the inequality

$$ab \leqslant \frac{1}{2}(a^2 + b^2), a, b \in \mathbf{R}, \tag{83}$$

for any $\xi \in \mathbf{R}, \xi > 0$,

$$\|\Psi_1\|\|\boldsymbol{z}_2\| = \|\Psi_1\|\xi^{\frac{1}{2}}\xi^{-\frac{1}{2}}\|\boldsymbol{z}_2\| \leqslant \frac{1}{2}\xi\|\Psi_1\|^2 + \frac{1}{2}\xi^{-1}\|\boldsymbol{z}_2\|^2. \tag{84}$$

substituting it into Equation (82), we have

$$\begin{aligned}\Gamma(\boldsymbol{z}, t) \leqslant & -\lambda_3^1\|\boldsymbol{z}_1\|^2 - \gamma_1\|\Psi_1\|^2 + \frac{1}{2}\xi\|\Psi_1\|^2 \\ & + \frac{1}{2}\xi^{-1}\|\boldsymbol{z}_2\|^2 - \lambda_3^2\|\boldsymbol{z}_2\|^2 + 2\varepsilon_1 + \frac{\varepsilon_2(1+\eta_{E_2})}{4} \\ = & -\left(\lambda_3^2 - \frac{1}{2}\xi^{-1}\right)\|\boldsymbol{z}_2\|^2 - \left(\gamma_1 - \frac{1}{2}\xi\right)\|\Psi_1\|^2 \\ & - \lambda_3^1\|\boldsymbol{z}_1\|^2 + 2\varepsilon_1 + \frac{\varepsilon_2(1+\eta_{E_2})}{4}.\end{aligned} \tag{85}$$

By choosing $\frac{1}{2\lambda_3^2} < \xi < 2\gamma_1$ and $\lambda_3^1 > 0$, we have

$$\Gamma(\boldsymbol{z}, t) \leqslant -\bar{\lambda}_3^1\|\boldsymbol{z}_1\|^2 - \bar{\lambda}_3^2\|\boldsymbol{z}_2\|^2 + 2\varepsilon_1 + \frac{\varepsilon_2(1+\eta_{E_2})}{4}, \tag{86}$$

where

$$\bar{\lambda}_3^1 = \lambda_3^1, \bar{\lambda}_3^2 = \lambda_3^2 - \frac{1}{2}\xi^{-1}. \tag{87}$$

Let

$$\begin{aligned}\hat{\lambda}_1(\|\boldsymbol{z}\|) &= \min\left\{\lambda_1^1\|\boldsymbol{z}_1\|, \lambda_1^2\|\boldsymbol{z}_2\|\right\}, \\ \hat{\lambda}_2(\|\boldsymbol{z}\|) &= \max\left\{\lambda_2^1\|\boldsymbol{z}_1\|, \lambda_2^2\|\boldsymbol{z}_2\|\right\}.\end{aligned} \tag{88}$$

□

According to Equation (86), by the literature, the practical stability of the system described by the Theorem 2 is guaranteed, the details are as follows:

I. The reconfigured system presents uniform boundedness, for any $\rho_z > 0$, if $\|\boldsymbol{z}(t_0)\| \leqslant \rho_z$, there exists

$$\chi_z(\rho_z) = \begin{cases}\left(\lambda_1^{-1} \circ \lambda_2\right)(\rho_z), & \text{if } \rho_z > P_z, \\ \left(\lambda_1^{-1} \circ \lambda_2\right)(P_z), & \text{if } \rho_z \leqslant P_z,\end{cases} \tag{89}$$

where

$$P_z = \sqrt{\left(2\varepsilon_1 + \frac{\varepsilon_2(1+\eta_{E_2})}{4}\right)\lambda_3^{-1}}, \tag{90}$$

to make $\|\boldsymbol{z}(t)\| \chi_z(\rho_z)$ for all tt_0.

II. The reconfigured system presents uniform ultimate boundedness: For any $\bar{\chi}_z$, satisfying

$$\bar{\chi}_z > \left(\lambda_1^{-1} \circ \lambda_2\right)(P_z), \tag{91}$$

when $t \geqslant t_0 + T_z(\bar{\chi}_z, \rho_z)$, $\|\boldsymbol{z}(t)\| \bar{\chi}_z$, where

$$T_z(\bar{\chi}_z, \rho_z) = \begin{cases}0, & \text{if } \rho_z \leqslant \bar{P}_z, \\ \dfrac{\lambda_2(\rho_z) - \lambda_1(\bar{P}_z)}{\lambda_3(\bar{P}_z) - \left[2\varepsilon_1 + \dfrac{\varepsilon_2(1+\eta_{E_2})}{4}\right]}, & \text{otherwise},\end{cases} \tag{92}$$

$$\bar{P}_z = \left(\lambda_2^{-1} \circ \lambda_1\right)(\bar{\chi}_z). \tag{93}$$

III. When $\phi_z(\bar{\chi}_z) = P_z$ is selected, the reconfigured system presents uniform stability.

Remark 5. The robust backstepping controller proposed in this paper enables the reconfigured systems (i.e., systems $\hat{N}_1$ and $\hat{N}_2$) to exhibit practical stability (including uniform boundedness, uniform ultimate boundedness, and uniform stability) under uncertainty disturbances.

4.3 | Stability Analysis of the Original System

In Sections 5.1 and 5.2, the robust backstepping controller (67) for the reconfigured system (79) is proposed, and the stability of the reconfigured system is proved theoretically. However, the actual controlled system is the tank VESS (32), and the goal is to design an appropriate controller to make it exhibit the expected characteristics, so the stability of the tank VESS under the action of the proposed robust backstepping controller is further analyzed.

Theorem 3. *Under the action of the controller $u(t)$, the original tank VESS presents practical stability (including uniform boundedness, uniform ultimate boundedness, and uniform stability). At the same time, by adjusting the control design parameters ε_i, $i = 1, 2$, the size of the region of uniform ultimate boundedness and uniform stability can be made infinitesimal.*

Proof. At first, supposing the boundary of $\boldsymbol{z}$ is κ, that is, $\|\boldsymbol{z}\| \leqslant \kappa$. According to $\boldsymbol{z} = [\boldsymbol{z}_1, \boldsymbol{z}_2]^{\mathrm{T}}$, we have

$$\|\boldsymbol{z}\|^2 = \|\boldsymbol{z}_1\|^2 + \|\boldsymbol{z}_2\|^2 \leqslant \kappa^2. \tag{94}$$

with Equation (78)

$$\|\boldsymbol{x}_1\| \leqslant \kappa, \|\boldsymbol{x}_2 - \boldsymbol{\nu}\| \leqslant \kappa. \tag{95}$$

Since

$$\boldsymbol{x}_2 = \boldsymbol{z}_2 + \boldsymbol{\nu} = \boldsymbol{z}_2 + \boldsymbol{\mu}_1(\boldsymbol{x}_1(t), t) - \gamma_1\boldsymbol{P}^{\mathrm{T}}\nabla_{\boldsymbol{x}_1}V_1(\boldsymbol{x}_1, t), \tag{96}$$

we have

$$\begin{aligned}\|\boldsymbol{x}_2\| &\leqslant \|\boldsymbol{z}_2\|+\|\boldsymbol{\mu}_2\|+\|\gamma_1 \boldsymbol{P}^{\mathrm{T}} \nabla_{\boldsymbol{x}_1} V_1(\boldsymbol{x}_1, t)\| \\ &\leqslant \|\boldsymbol{z}_2\|+\|\boldsymbol{\mu}_2\|+\gamma_1\|\boldsymbol{P}^{\mathrm{T}}\|\|\nabla_{\boldsymbol{x}_1} V_1(\boldsymbol{x}_1, t)\|,\end{aligned} \tag{97}$$

recalling $\|\boldsymbol{\mu}_2\| \leqslant \|\mu_{11}\| \leqslant \eta_{\boldsymbol{q}_1}$ and Equation (35), we have

$$\|\boldsymbol{x}_2\| \leqslant \|\boldsymbol{z}_2\| + \eta_{\boldsymbol{q}_1} + \gamma_1\|\boldsymbol{P}^{\mathrm{T}}\|\lambda_4^1(\|\boldsymbol{x}_1\|), \tag{98}$$

since $\eta_{\boldsymbol{q}_1}(\cdot)$ and $\lambda_4^1(\cdot)$ are the continuous functions, and $\eta_{\boldsymbol{q}_1}(0) = 0$, $\lambda_4^1(0) = 0$, if $\|\boldsymbol{x}_1\| \leqslant \kappa$ and $\|\boldsymbol{x}_2\| \leqslant \kappa$, existing the constants $r_1(\kappa)$ and $\tilde{r}_1(\kappa)$ to make (where $\gamma_1 < \infty$)

$$\|\boldsymbol{x}_2\| \leqslant \kappa + r_1(\kappa) + \gamma_1 b_1 \tilde{r}_1(\kappa), \tag{99}$$

where

$$b_1 \coloneqq \sup_{\|\boldsymbol{x}_1\| \leqslant \kappa} \|\boldsymbol{P}^{\mathrm{T}}\|. \tag{100}$$

The boundedness of $\boldsymbol{x}_{1,2}$ can be described as

$$\|\boldsymbol{x}_1\| \leqslant \kappa_1, \ \|\boldsymbol{x}_2\| \leqslant \kappa_2, \tag{101}$$

where

$$\begin{aligned}&\kappa_1 \coloneqq \kappa, \\ &\kappa_2 \coloneqq \kappa + r_1(\kappa) + \gamma_1 b_1 \tilde{r}_1(\kappa).\end{aligned} \tag{102}$$

□

It can be seen that if $\mathbf{P}(\cdot)$ is continuous, then b_1 is bounded. This implies that if $\mathbf{x}_1$ and $\mathbf{z}_2$ are bounded, then $\mathbf{x}_2$ is bounded. Furthermore, if $\kappa \to 0$, then there are $r_1(\kappa) \to 0$ and $\tilde{r}_1(\kappa) \to 0$.

For any $a \geqslant 0$, the following definition is made

$$\begin{aligned}&I_1(a) \coloneqq a, \\ &I_2(a) \coloneqq a + r_1(a) + \gamma_1 b_1 \tilde{r}_1(a), \\ &\omega(a) = \sqrt{I_1(a) + I_2(a)}.\end{aligned} \tag{103}$$

According to Theorem 2, when $\mathbf{z}(t)$ is uniformly bounded, $\|\mathbf{z}(t)\| \leqslant \chi_z(\rho_z)$ for any $t \geqslant t_0$. By replacing κ with $\chi_z(\rho_z)$, Equation (101) can be rewritten as

$$\begin{aligned}&\|\boldsymbol{x}_1(t)\| \leqslant \chi_z(\rho_z), \\ &\|\boldsymbol{x}_2(t)\| \leqslant \chi_z(\rho_z) + r_1(\chi_z(\rho_z)) + \gamma_1 b_1^{\chi_z(\rho_z)} \tilde{r}_1(\chi_z(\rho_z)).\end{aligned} \tag{104}$$

So

$$\|\mathbf{x}(t)\| \leqslant \omega(\chi_z(\rho_z)). \tag{105}$$

From the above analysis, it can be seen that when the reconfigured system state variable $\boldsymbol{z}(t)$ is uniformly bounded, the original system state variable $\boldsymbol{x}(t)$ also presents uniform boundedness. For any $\rho_z > 0, \|\boldsymbol{z}(t_0)\| \leqslant \rho_z$, there exists $\rho_x = \omega(\rho_z) > 0$ where $\|\boldsymbol{x}(t_0)\| \leqslant \rho_x$, $\|\boldsymbol{z}(t)\| \leqslant \chi_z(\rho_z)$, it means that $\|\boldsymbol{x}(t)\| \leqslant \chi_x(\rho_x)$. Let $\chi_x = \omega(\underline{\chi}_z)$, $\boldsymbol{x}(t)$ presents uniform ultimate boundedness: For any $\bar{\chi}_x > \underline{\chi}_x$, there exists $T_x(\bar{\chi}_x, \rho_x) < \infty$, then $\|\boldsymbol{x}(t)\| \leqslant \bar{\chi}_x$ for all $t \geqslant t_0 + T_x(\bar{\chi}_x, \rho_x)$. Finally, when choosing

$$\phi_x(\bar{\chi}_x) = P_x = \omega(P_z), \tag{106}$$

the original system presents uniform stability.

Furthermore, according to Equations (89) and (93), when choose the control parameters $\varepsilon_{1,2} \to 0$, then $P_z \to 0, \chi_z(\rho_z) \to 0, \bar{\chi}_z \to 0$, thus $\chi_x(\rho_x) = \omega(\chi_z(\rho_z)) \to 0, \bar{\chi}_x = \omega(\bar{\chi}_z) \to 0$. In summary, when the reconfigured system presents practical stability, the original system equally presents practical stability. At the same time, by adjusting the control design parameters $\varepsilon_i, i = 1, 2$, the size of the region of uniform ultimate boundedness and uniform stability can be made infinitesimal.

Remark 6. For the problem of tank pitch-pointing tracking control, the original controlled system is reconstructed by system state transformation to make the reconfigured system a matched uncertain system to deal with the mismatched uncertainty of the VESS. Thus, the robust backstepping controller is designed. Under the action of this controller, both the reconfigured system and the original VESS can present practical stability, which makes the pitch angle of barrel $\varphi_r(t)$ track approximately the desired reference signal, thus realizing the tank pitch-pointing tracking control.

5 | Controller Design Ideas and Processes

To effectively suppress the coupling influence of the complex flexible nonlinearity and two types of uncertainty (matched uncertainty and mismatched uncertainty) of the VESS, a novel robust backstepping control strategy is proposed. As shown in Figure 6, the design flow of the proposed robust backstepping control method can be summarized as follows:

i. Analyze the complex, flexible nonlinearity of tank VESS and consider the dynamics of the control actuator under fully electric drive. Based on the axial stiffness model of the electric cylinder and the modal solution of the flexible barrel, the coupling dynamics model of VESS is established (20).

ii. Study the mathematical description method of tank pitch-pointing tracking control, the tracking error of the barrel pitch angle $e(t)$ is defined as the control tracking object; describe the coupling dynamics model in the state space of tank VESS (20), considering the matched and mismatched uncertainty; construct the mismatched state space model (32) as the controlled system.

iii. Choose the appropriate functions $\bar{g}_{12}(\cdot)$ and $\bar{g}_{22}(\cdot)$ to make the uncontrolled nominal system present uniform asymptotically stable at the origins; meanwhile, choose the appropriate functions $\lambda_{1,2,3}^1(\cdot), \lambda_{1,2,3}^2(\cdot), V_{1,2}(\cdot)$ to satisfy Equations (33) and (34). Analyze the boundary conditions of the uncertain part $\Delta\mathbf{g}_1$ of the VESS to obtain η_{q_1}, as shown in Equation (41), and select the control parameter ε_1, which leads to the design of the implanted robust controller $\boldsymbol{\nu}(t)$, as shown in Equation (49).

iv. Analyze the boundary conditions of uncertain part $\Delta\mathbf{a}_2$ of the reconfigured system to obtain η_{q_2}, as shown in Equation (66)

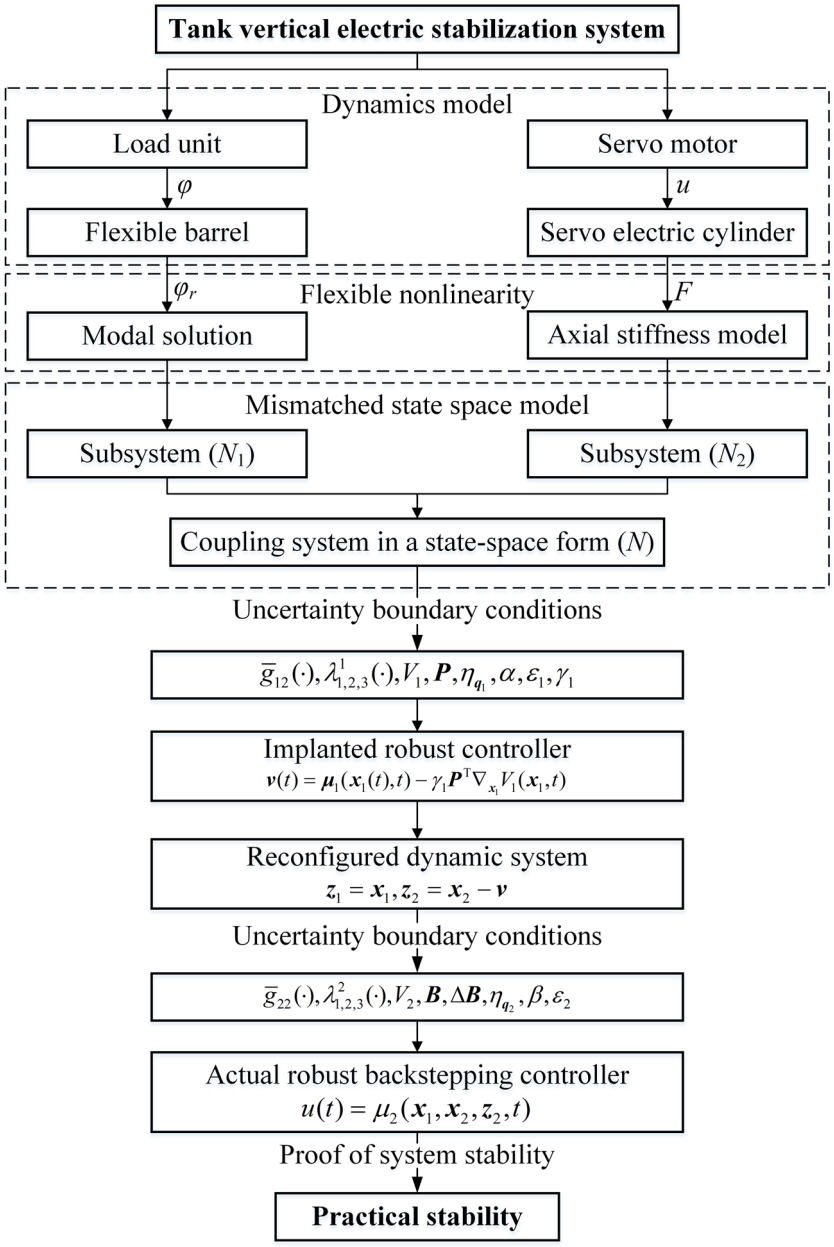

FIGURE 6 | The design flow of the proposed robust backstepping control method.

and select the control parameters ε_2, which leads to the actual robust backstepping controller $u(t)$, as shown in Equation (67). According to the practical stability theory described in Theorems 2 and 3, the practical stability of the reconfigured system and the original system is proved.

6 | Simulation Analysis

6.1 | Parameter Selections

In the simulation, two different desired reference signals are considered for validating the steady-state tracking performance and stability, as well as the dynamic tracking performance and stability of the designed controller. In Simulation I, the pitch angle of barrel is set to adjust from $\varphi_r(t) = 0$ rad to $\varphi_r(t) = 0.1$ rad for validating the steady-state comprehensive performance of the controller, so the desired reference signal is set as $\varphi_d(t) = 0.1$ rad, thus, the initial tracking errors $e(0) = -0.1$ rad (i.e., $x_{11}(0) = -0.1$) and the initial thrust of the electric cylinder $F(0) = 0\ N$ (i.e., $x_{21}(0) = 0$). Meanwhile, the other initial states are set as $x_{12}(0) = 0$ and $x_{22}(0) = 0$. In Simulation II, the pitch angle of barrel is set to adjust from $\varphi_r(t) = -0.1$ rad to $\varphi_r(t) = 0.1 \times \sin(0.2\pi t)$ rad for validating the dynamic comprehensive performance of the controller, so the desired reference signal is set as $\varphi_d(t) = 0.1 \times \sin(0.2\pi t)$ rad, thus, the initial tracking errors $e(0) = -0.1$ rad (i.e., $x_{11}(0) = -0.1$) and the initial thrust of the electric cylinder $F(0) = 0\ N$ (i.e., $x_{21}(0) = 0$). Meanwhile, the other initial states are set as $x_{12}(0) = 0$ and $x_{22}(0) = 0$.

Then, the system modeling error and external disturbance are considered as system uncertainty to validate the suppression effect of the proposed control method on the complex

time-varying uncertainty. For system modeling error, according to the electric cylinder model parameters and past experimental results, choose the axial stiffness of the electric cylinder $k_{se} = 3.4 \times 10^8 + 0.15 \times 10^8 \times \sin(10t)\,\mathrm{N/m}$, for external disturbance. Based on the vibration data of the tank traveling on the complex road, approximately choose the external disturbance torque $f_d = 10 \times \sin(10t)\,\mathrm{N\,m}$.

Next, recalling the design process of the proposed controller, it is necessary to choose appropriate functions $\bar{g}_{12}$ and $\bar{g}_{22}$ to make the uncontrolled nominal system $\boldsymbol{x}_1 = \boldsymbol{g}_1(\boldsymbol{x}_1, t)$ and $\boldsymbol{x}_2 = \boldsymbol{g}_2(\boldsymbol{x}_2, t)$ present uniform asymptotically stable at the origins (i.e., $\boldsymbol{x}_{1,2} = 0$). Assuming $\bar{g}_{12} = -a_1 x_{11} - b_1 x_{12}, \bar{g}_{22} = -a_2 x_{21} - b_2 x_{22}$, thus $g(\boldsymbol{z}_2) = -a_2 z_{21} - b_2 z_{22}$, according to Equation (32), the uncontrolled nominal system can be expressed as

$$\begin{aligned} \dot{\boldsymbol{x}}_1 &= \boldsymbol{A}_1 \boldsymbol{x}_1, \\ \dot{\boldsymbol{x}}_2 &= \boldsymbol{A}_2 \boldsymbol{x}_2, \end{aligned} \tag{107}$$

where $\boldsymbol{A}_1 = [0\ 1; -a_1\ \ -b_1]$, $\boldsymbol{A}_2 = [0\ 1; -a_2\ \ -b_2]$, according to Equations (33)–(35), choose $\boldsymbol{V}_1 = \boldsymbol{x}_1^{\mathrm{T}} \boldsymbol{G}_1 \boldsymbol{x}_1$ and $\boldsymbol{V}_2 = \boldsymbol{x}_2^{\mathrm{T}} \boldsymbol{G}_2 \boldsymbol{x}_2$. Choose $a_{1,2} = 1$ and $b_{1,2} = 2$, so $\boldsymbol{A}_{1,2} = [0\ 1; -1\ \ -2]$, choose $\boldsymbol{Q} = [2\ 0; 0\ 2]$, through Lyapunov equation

$$\boldsymbol{A}^{\mathrm{T}} \boldsymbol{G} + \boldsymbol{G}\boldsymbol{A} + \boldsymbol{Q} = 0, \tag{108}$$

$\boldsymbol{G}_{1,2} = [3\ 1; 1\ 1]$ can be obtained.

Finally, in the simulation, the parameters of the flexible barrel are set as $m = 2370$ kg, $g = 9.8\,\mathrm{N/kg}$, $E = 2.4 \times 10^{11}\,\mathrm{Pa}$, $I = 6.4 \times 10^{-5}\,\mathrm{kg\,m^2}$, $\rho = 7800\,\mathrm{kg/m^2}$, $A = 0.028\,\mathrm{m^2}$, $L_1 = 0.89$ m, $L_2 = 4.46$ m, the parameters of the servo motor and the electric cylinder are set as $k_t = 1.632\,\mathrm{N\,m/A}$, $k_e = 1.605\,\mathrm{V\,s/rad}$, $R = 1.15\,\Omega$, $J_{eq} = 0.21\,\mathrm{kg\,m^2}$, $B_{eq} = 0.0675\,\mathrm{N\,m/rad}$, $P_h = 0.016$ m, $i = 4$, and the installation parameters of the electric cylinder are set as $d_0 = 0.4$ m, $l_1 = 0.3$ m, $l_2 = 0.1$ m, $l_3 = 0.5$ m, $\theta_0 = 0.92$ rad.

To better verify the effectiveness of the proposed pitch-pointing tracking control method of the VESS, the PID controller and sliding mode controller (SMC controller) are selected for comparisons with the proposed controller in the simulation process. For a PID controller, the control input can be designed as

$$u(t) = k_p e(t) + k_i \int_0^t e(\tau)\mathrm{d}\tau + k_d \frac{\mathrm{d}e(t)}{\mathrm{d}t}. \tag{109}$$

For SMC controller, the control input can be designed as

$$u(t) = -\iota sat\left(\frac{e(t)}{\Xi}\right), \tag{110}$$

where

$$sat\left(\frac{e(t)}{\Xi}\right) = \begin{cases} 1, & \frac{e(t)}{\Xi} > 1, \\ \frac{e(t)}{\Xi}, & -1 \leqslant \frac{e(t)}{\Xi} \leqslant 1, \\ -1, & \frac{e(t)}{\Xi} < -1, \end{cases} \tag{111}$$

where k_p, k_i, k_d, ι, Ξ are the design parameters.

Remark 7. The reasons for selecting PID control and SMC control are: (1) at this stage, the traditional tank fire control system adopts PID control, which is of more practical significance for comparison; (2) SMC control is a class of advanced nonlinear control methods, which has the advantages of fast response, insensitivity to parameter changes and perturbations, no requirement for online identification of the system, and simple physical realization, and so forth, which can further verify the effectiveness of the proposed control algorithms by selecting it for comparison.

In Simulation I, the control design parameters of the proposed controller are set as $\varepsilon_1 = 250$, $\varepsilon_2 = 1$, $\gamma_1 = 0.001$, for the PID controller, $k_p = -60$, $k_i = -0.4$, $k_d = -175$, for the SMC controller, $\Xi = 0.07$, $\iota = 9000$. In Simulation II, the control design parameters of the proposed controller are set as $\varepsilon_1 = 600$, $\varepsilon_2 = 1$, $\gamma_1 = 0.001$, for the PID controller, $k_p = -65$, $k_i = -0.5$, $k_d = -160$, and for the SMC controller, $\Xi = 0.075$, $\iota = 8000$.

The determination of control parameters in this study was guided by a combination of theoretical analysis and simulation-based optimization. The backstepping design provides theoretical guidelines for selecting parameter ranges, while simulation experiments were conducted to fine-tune these parameters for optimal performance. Specifically, the parameters ε_1, ε_2, and γ_1 were adjusted to balance the trade-off between control accuracy, robustness, and stability. For example, ε_1 and ε_2 were tuned to minimize the tracking error while ensuring robustness to uncertainties, and γ_1 was optimized to guarantee stability during the state variable transformation process. This two-step approach ensures that the control parameters are both theoretically sound and practically effective.

6.2 | Simulation Results

The simulation results are presented in two distinct scenarios, each with different desired signals, as shown in Figures 7–10 and 11–14, respectively.

In Simulation I, Figures 7 and 8 illustrate the comparative tracking error e and the comparative pitch angle of the barrel φ_r. It is evident that under the proposed control method, the tracking error e converges from −0.1 rad to 0 rad within approximately 5 s and stabilizes near 0 rad. Similarly, the pitch angle of the barrel φ_r converges and stabilizes near the desired angle $\varphi_d = 0.1$ rad after 5 s. In contrast, both PID control and SMC exhibit longer convergence times and significant fluctuations around zero in the steady state. Furthermore, the pitch angle of the barrel φ_r takes considerably longer to converge and stabilize near the desired angle, with a maximum steady-state error of up to 0.08 rad. These results highlight the superior accuracy and stability of the proposed control method compared to PID and SMC.

Figures 9 and 10 depict the comparative thrust of the electric cylinder F and the comparative control input voltage u, respectively. With the proposed control, once the pitch angle of the barrel φ_r stabilizes around the desired angle (after approximately 5 seconds), both the thrust of the electric cylinder F and

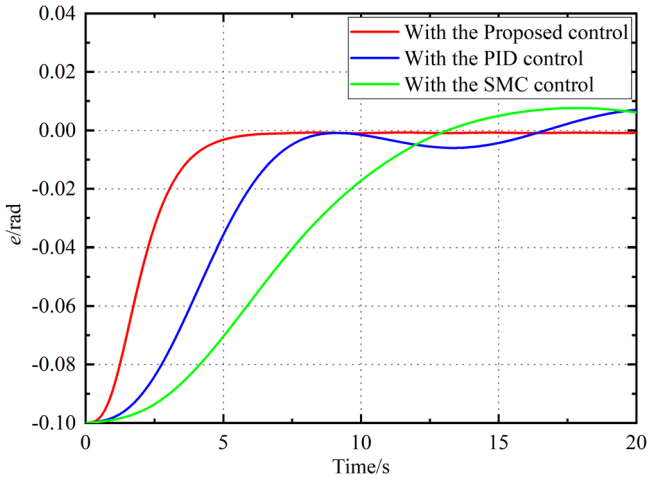

FIGURE 7 | Comparative tracking error e in Simulation I.

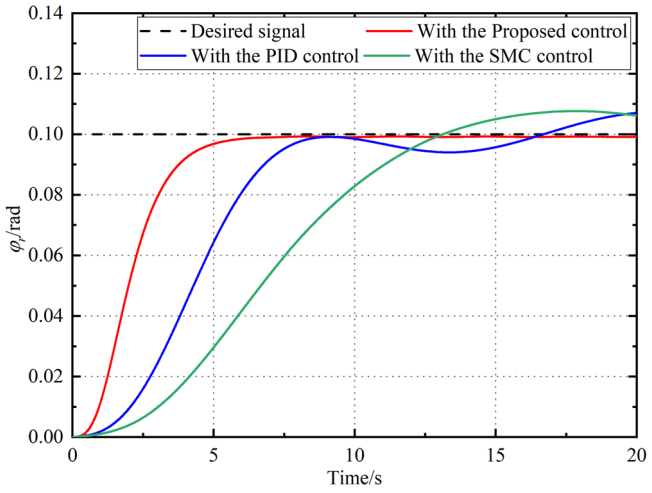

FIGURE 8 | Comparative pitch angle of barrel φ_r in Simulation I.

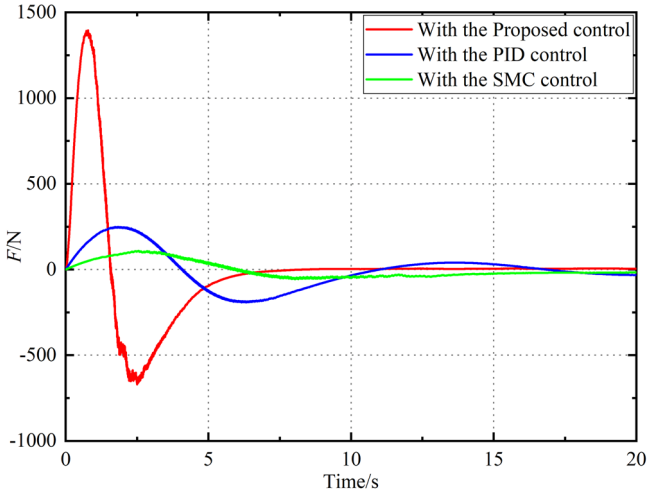

FIGURE 9 | Comparative thrust of electric cylinder F in Simulation I.

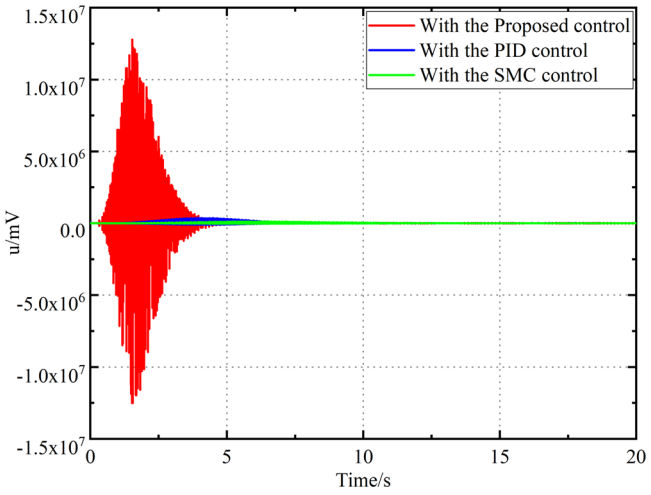

FIGURE 10 | Comparative control input voltage u in Simulation I.

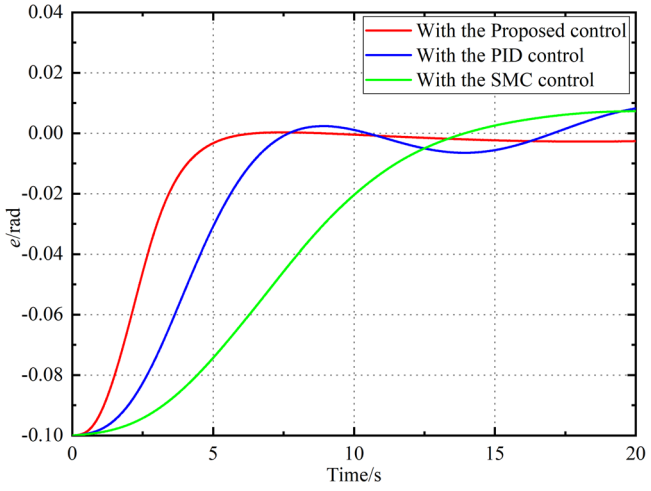

FIGURE 11 | Comparative tracking error e in Simulation II.

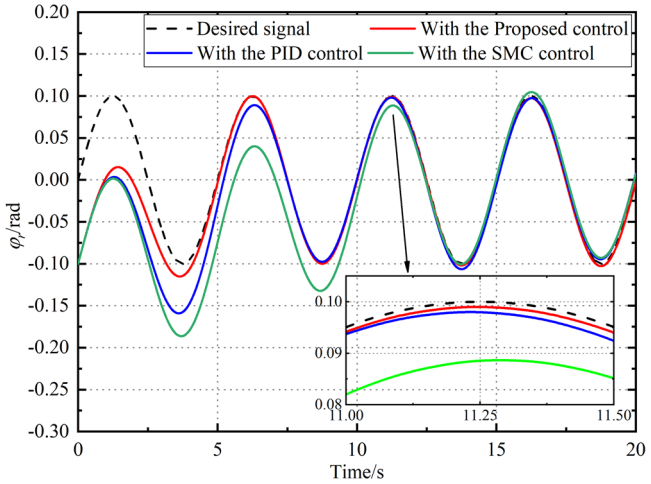

FIGURE 12 | Comparative pitch angle of barrel φ_r in Simulation II.

the control input voltage u reach a stable state, indicating that the entire VESS achieves stability. In contrast, under PID and SMC control, the thrust of the electric cylinder F and the control input voltage u exhibit continuous fluctuations, making it difficult for the system to reach a steady state.

In Simulation II, Figures 11 and 12 present the comparative tracking error e and the comparative pitch angle of the barrel φ_r, respectively, while Figures 13 and 14 show the comparative thrust of the electric cylinder F and the comparative control input voltage u. The results are consistent with those of

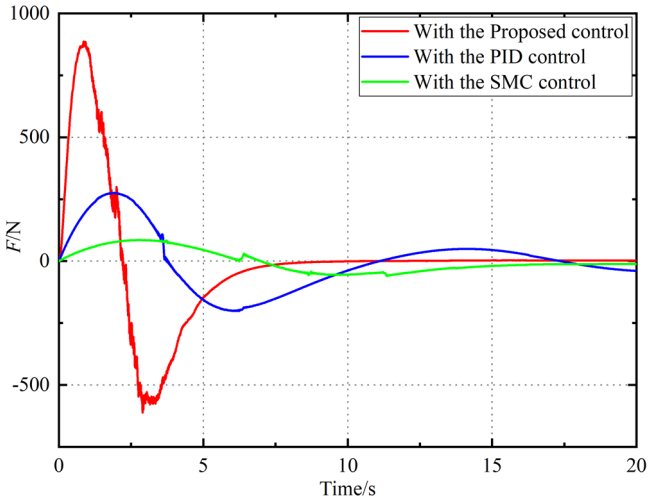

FIGURE 13 | Comparative thrust of electric cylinder F in Simulation II.

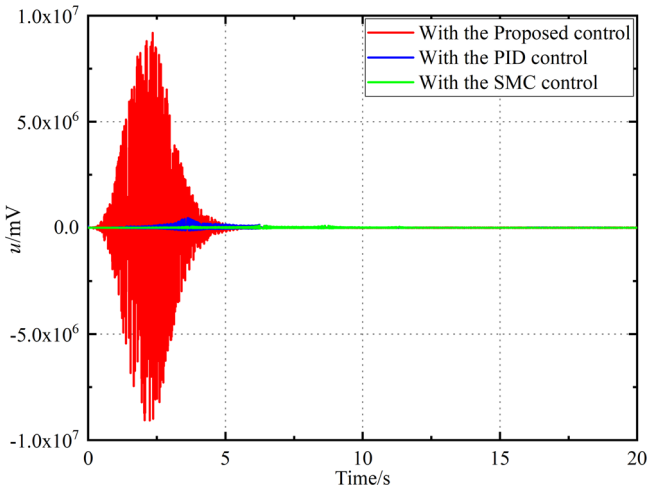

FIGURE 14 | Comparative control input voltage u in Simulation II.

Simulation I, further validating the accuracy and stability of the proposed control method in dynamic tracking processes. Notably, the influence of system uncertainty and nonlinearity becomes more pronounced when the desired signal is dynamic. Traditional PID and SMC controls fail to effectively suppress nonlinear disturbances, whereas the proposed control method demonstrates superior performance in handling system uncertainty and nonlinearity.

From the simulation results, it is clear that the proposed control strategy effectively addresses the complex flexible nonlinearity and two types of uncertainty (matched and mismatched) in the VESS. However, it is worth noting that the proposed method requires larger control inputs during the initial stage to counteract the system's nonlinearity and uncertainty. This initial demand for higher control effort is a trade-off for achieving enhanced stability and accuracy in the steady state. Overall, the proposed control method outperforms traditional approaches in terms of convergence speed, steady-state accuracy, and robustness under dynamic conditions.

7 | Experimental Validation

7.1 | Composition Introduction

The experimental platform, constructed using the scaling theory of VESS, is mainly composed of mechanical, electrical, and testing components [13]. The platform's mechanical part mimics the upper structure of a tank, primarily consisting of the gun breech, cradle, front bush, rear bush, and barrel. In addition to the electrical part of the platform, which is electrically controlled by a servo motor and an electric cylinder, enabling the stabilized pitch motion of the tank barrel. The control equipment manages the pitch motion of the test stand as well as its parameter settings. The platform employs a TMS320F283325 DSP with a main frequency of 150 MHz. Parameters such as the working mode, desired angle, and desired angular speed are set through the HMI control interface, after which the electrical equipment must function according to the parameter settings and complete the pitch motion function. The testing part, on the other hand, consists of an inclination sensor mounted on the muzzle, an angle encoder mounted on the trunnion, and a force sensor mounted on the electric cylinder actuator, which realizes the closed-loop control of the vertical electric stabilization system by means of the data from the sensors. Besides, the platform uses a shaking table to simulate the excitation caused by road roughness, with an adjustable weight design featured in the gun breech. External interfaces all use a common interface; the console integrates a certain number of network interfaces, asynchronous serial interfaces, and image interfaces, facilitating the data exchange and information transmission of the test stand.

In the experiment, the shaking table data is set to be saddle ring vibration data of a tank moving at 30 km/h on a Class D road, so as to simulate the driving conditions of a tank moving at 30 km/h on a Class D road. The dynamic parameters of the experimental platform are given in Table 1, and the PID and the SMC are still introduced as the comparison method.

7.2 | Experimental Results

For the same purpose of the simulation, the desired reference signal is set as $\varphi_d(t) = 0.021 \times (1 - e^{-0.1t^3})$ rad and $\varphi_d(t) = 0.021 \times \sin(0.4\pi t)$ in Experiments I and II, respectively.

The comparative tracking error e and the comparative pitch angle of barrel φ_r in Experiment I are, respectively, shown in Figures 15 and 16. From the experimental results, under the three different control strategies, the system stabilizes in approximately the same time. However, compared to the proposed control, under SMC control, the system always vibrates after stabilization with a large amplitude, and under PID control, the system tends to stabilize at a value that is still somewhat different from the target value. The comparative tracking error e and the comparative pitch angle of barrel φ_r in Experiment II are, respectively, shown in Figures 18 and 19. The experimental results similarly show that the proposed control has

TABLE 1 | Dynamic physical parameters of the experimental platform.

Parameter	Value	Unit
m	71.01	kg
g	9.8	m/s^2
J_{eq}	2.39×10^{-3}	kgm^2
i	36	—
B_{eq}	3.375×10^{-4}	Nms/rad
P_{h}	0.008	m
k_{e}	0.285	Vs/rad
k_{t}	0.185	Nm/A
R	0.55	Ω
L_2	1.633	m
l_1	0.094	m
l_2	0.042	m
l_3	0.194	m
d_0	0.170	m
φ	1.065	rad

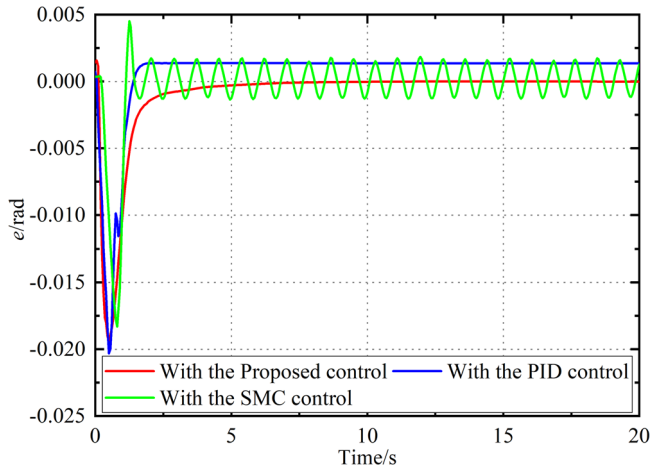

FIGURE 15 | Comparative tracking error e in Experiment I.

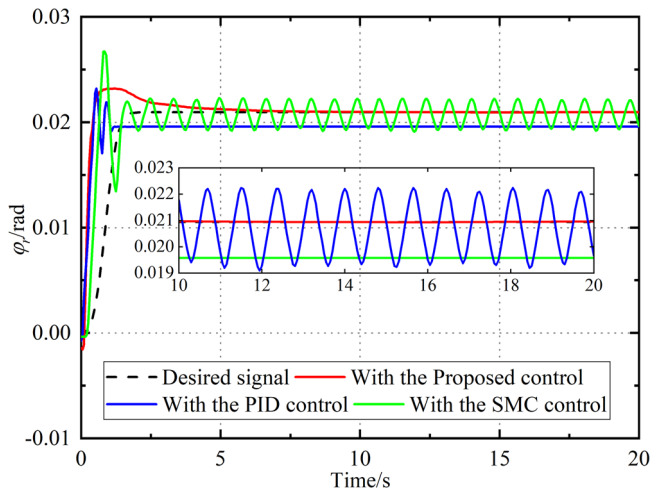

FIGURE 16 | Comparative pitch angle of barrel φ_r in Experiment I.

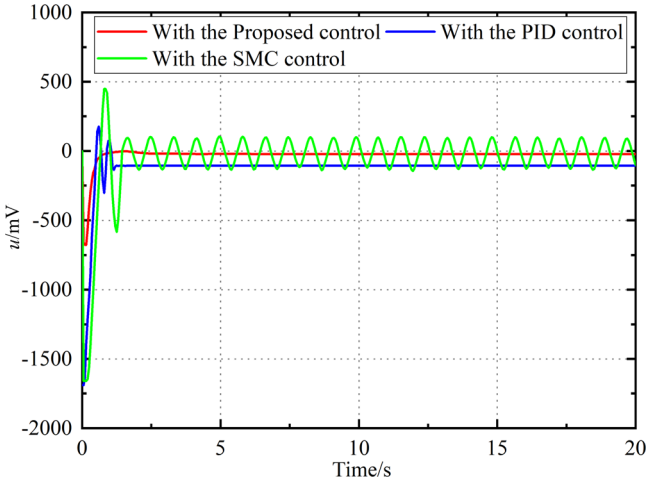

FIGURE 17 | Comparative control input voltage u in Experiment I.

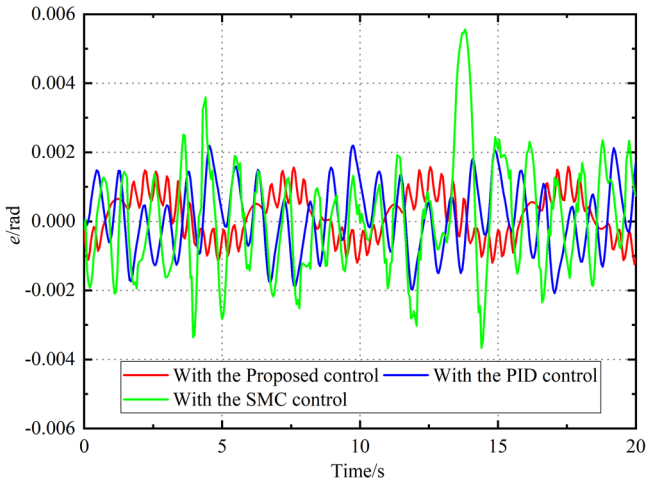

FIGURE 18 | Comparative tracking error e in Experiment II.

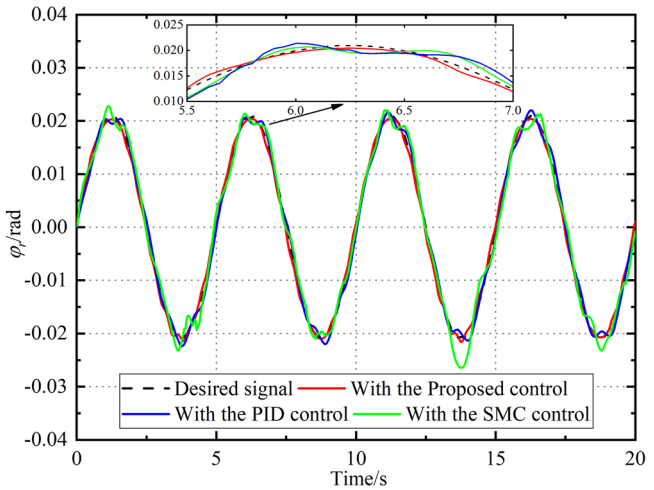

FIGURE 19 | Comparative pitch angle of barrel φ_r in Experiment II.

better dynamic tracking performance relative to the PID and SMC controls. The comparative control input voltage u in Experiments I and II are, respectively, shown in Figures 17 and 20. The change rule of the control input voltage u basically keeps

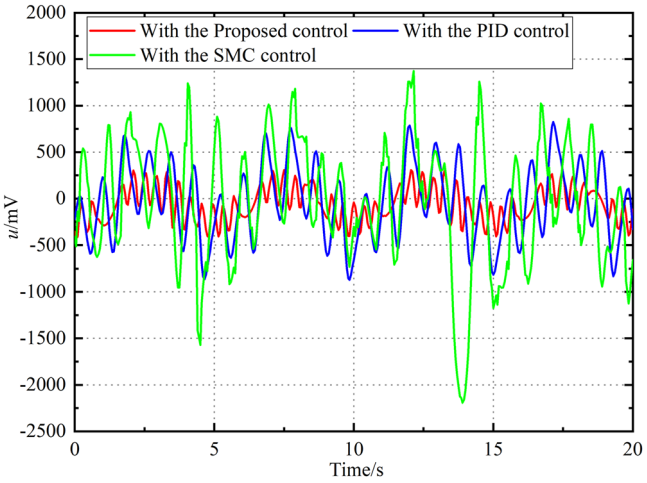

FIGURE 20 | Comparative control input voltage u in Experiment II.

the same trend with the corresponding error curve, characterizing the reasonableness and effectiveness of the control strategy verified by this experimental platform; moreover, the control voltage also presents a stable state after the system tends to be stabilized under the proposed control strategy.

8 | Conclusion

To enhance the stability and accuracy of pitch-pointing tracking control, this study proposes a novel robust backstepping control strategy that explicitly incorporates flexible nonlinearity and mismatched uncertainty into the dynamics modeling process of the VESS. The research framework is structured as follows: First, a nonlinear coupled dynamics model is established by integrating the axial stiffness model of the electric cylinder with the modal solution of the flexible barrel, thereby capturing the system's flexible coupling effects. Second, to address both matched and mismatched uncertainties, a mismatched state space model, which consists of two interconnected subsystems, is developed. Third, through the application of backstepping design principles, a state variable transformation is implemented to convert the mismatched uncertainty boundary, leading to the development of an innovative robust control method. This approach guarantees practical stability for both the original and reconfigured systems. Extensive simulation and experimental results demonstrate the superior performance of the proposed method compared to traditional control approaches. Notably, this study represents the first attempt to introduce flexible nonlinearity into the pitch-pointing tracking problem of VESS, offering a groundbreaking perspective for future research in this domain.

However, the method relies on accurate modeling of flexible nonlinearities and uncertainties, which can be challenging to achieve in real-world scenarios with limited sensor data and changing environmental conditions. Secondly, the computational complexity of the control algorithm may increase the system control cost. Future research is expected to develop data-driven modeling techniques to reduce the reliance on precise analytical models. Further bridge the gap between theoretical research and practical application.

Conflicts of Interest

The authors declare no conflicts of interest.

Data Availability Statement

The data that support the findings of this study are available from the corresponding author upon reasonable request.

References

1. J. Zhu, B. Zhao, and Q. Wang, *Modern Tank Fire Control System* [in Chinese] (National Defense Industry Press, 2003).

2. T. Dursun, F. Büyükcivelek, and Ç. Utlu, "A Review on the Gun Barrel Vibrations and Control for a Main Battle Tank," *Defence Technology* 13, no. 5 (2017): 353–359.

3. F.-f. Liu, Y.-m. Song, H.-l. Yu, et al., "Study on the Influence of Projectile on Muzzle Disturbance," *Defence Technology* 14, no. 5 (2018): 570–577.

4. Y. Chen and G. Yang, "Dynamic Simulation of Tank Stabilizer Based on Adaptive Control," *Proceedings of the Institution of Mechanical Engineers, Part C: Journal of Mechanical Engineering Science* 233, no. 9 (2019): 3038–3049.

5. C. Li, G. Yang, X. Wang, Y. Ma, L. Wang, and Q. Sun, "Adaptive Robust Target Tracking Control of Marching Tank Under High-Speed Maneuvering Condition," *Journal of Mechanical Science and Technology* 36, no. 6 (2022): 2787–2798.

6. Y. Chen, G. Yang, and Q. Sun, "Dynamic Simulation on Vibration Control of Marching Tank Gun Based on Adaptive Robust Control," *Journal of Low Frequency Noise, Vibration and Active Control* 39, no. 2 (2020): 416–434.

7. S. S. Yuan, W. X. Deng, J. Y. Yao, and G. L. Yang, "Robust Adaptive Precision Motion Control of Tank Horizontal Stabilizer Based on Unknown Actuator Backlash Compensation," *Defence Technology* 20 (2023): 72–83.

8. C. Li, X. Wang, Y. Ma, F. Xu, and G. Yang, "The Prediction of Projectile-Target Intersection for Moving Tank Based on Adaptive Robust Constraint-Following Control and Interval Uncertainty Analysis," *Defence Technology* 31 (2024): 351–363.

9. Y. Chen and G. Leitmann, "Robustness of Uncertain Systems in the Absence of Matching Assumptions," *International Journal of Control* 45, no. 5 (1987): 1527–1542.

10. J. Yang, S. Li, and X. Yu, "Sliding-Mode Control for Systems With Mismatched Uncertainties via a Disturbance Observer," *IEEE Transactions on Industrial Electronics* 60, no. 1 (2012): 160–169.

11. Q. Sun, X. Wang, G. Yang, Y. H. Chen, and F. Ma, "Adaptive Robust Control for Pointing Tracking of Marching Turret-Barrel Systems: Coupling, Nonlinearity and Uncertainty," *IEEE Transactions on Intelligent Transportation Systems* 23, no. 9 (2022): 16397–16409.

12. Y.-z. Ma, G.-l. Yang, Q.-q. Sun, X.-y. Wang, and Z.-f. Wang, "Adaptive Robust Feedback Control of Moving Target Tracking for All-Electrical Tank With Uncertainty," *Defence Technology* 18, no. 4 (2022): 626–642.

13. D. Lin, X. Wang, Y. Wang, and G. Yang, "Adaptive Robust Servo Control for Vertical Electric Stabilization System of Tank and Experimental Validation," *Defence Technology* 31 (2024): 326–342.

14. Y. Zhang, Q. Yan, J. Cai, and X. Wu, "Adaptive Iterative Learning Control for Tank Gun Servo Systems With Input Deadzone," *IEEE Access* 8 (2020): 63443–63451.

15. D. X. Li, H. S. Yan, and T. Jin, "Multi-dimensional Taylor Network Optimal Control for Tank Firing in High Speed Motion," in *2017 IEEE 2nd Advanced Information Technology, Electronic and Automation Control Conference (IAEAC)* (IEEE, 2017), 961–965.

16. J. P. Cai and J. E. Ma, "Robust Adaptive Control for Gun Control System of Tank," *Advanced Materials Research* 295 (2011): 270–273.

17. J. Zhou and J. Yang, "Smooth Sliding Mode Control for Missile Interception With Finite-Time Convergence," *Journal of Guidance, Control, and Dynamics* 38, no. 7 (2015): 1311–1318.

18. S. Yuan, W. Deng, J. Yao, and G. Yang, "Robust Control for Bidirectional Stabilization System With Time Delay Estimation," *International Journal of Control, Automation and Systems* 22, no. 4 (2024): 1163–1175.

19. D. Zhang, Y. Wang, L. Meng, J. Yan, and C. Qin, "Adaptive Critic Design for Safety-Optimal FTC of Unknown Nonlinear Systems With Asymmetric Constrained-Input," *ISA Transactions* 155 (2024): 309–318.

20. C. Qin, X. Qiao, J. Wang, D. Zhang, Y. Hou, and S. Hu, "Barrier-Critic Adaptive Robust Control of Nonzero-Sum Differential Games for Uncertain Nonlinear Systems With State Constraints," *IEEE Transactions on Systems, Man, and Cybernetics: Systems* 54, no. 1 (2023): 50–63.

21. J. Wang, H. Pan, and D. Zhang, "Event-Triggered Adaptive Finite-Time Control for MIMO Nonlinear Systems With Actuator Faults," *IEEE Transactions on Industrial Electronics* 70, no. 7 (2022): 7343–7352.

22. J. Cai, R. Yu, Q. Yan, C. Mei, B. Wang, and L. Shen, "Event-Triggered Adaptive Control for Tank Gun Control Systems," *IEEE Access* 7 (2019): 17517–17523.

23. D. Yue, E. Tian, and Q. L. Han, "A Delay System Method for Designing Event-Triggered Controllers of Networked Control Systems," *IEEE Transactions on Automatic Control* 58, no. 2 (2012): 475–481.

24. B. Das and P. Mhaskar, "Adaptive Output-Feedback Lyapunov-Based Model Predictive Control of Nonlinear Process Systems," *International Journal of Robust and Nonlinear Control* 28, no. 5 (2018): 1597–1609.

25. M. Mahmood and P. Mhaskar, "Lyapunov-Based Model Predictive Control of Stochastic Nonlinear Systems," *Automatica* 48, no. 9 (2012): 2271–2276.

26. D. Angeli and E. Mosca, "Lyapunov-Based Switching Supervisory Control of Nonlinear Uncertain Systems," *IEEE Transactions on Automatic Control* 47, no. 3 (2002): 500–505.

27. D. Zhang, X. Hao, L. Liang, W. Liu, and C. Qin, "A Novel Deep Convolutional Neural Network Algorithm for Surface Defect Detection," *Journal of Computational Design and Engineering* 9, no. 5 (2022): 1616–1632.

28. D. Zhang, X. Hao, D. Wang, et al., "An Efficient Lightweight Convolutional Neural Network for Industrial Surface Defect Detection," *Artificial Intelligence Review* 56, no. 9 (2023): 10651–10677.

29. W. He, Y. Chen, and Z. Yin, "Adaptive Neural Network Control of an Uncertain Robot With Full-State Constraints," *IEEE Transactions on Cybernetics* 46, no. 3 (2015): 620–629.

30. B. Xu, "Composite Learning Control of Flexible-Link Manipulator Using NN and DOB," *IEEE Transactions on Systems, Man, and Cybernetics: Systems* 48, no. 11 (2017): 1979–1985.

31. Y. Yang, Z. Liu, and G. Ma, "Adaptive Distributed Control of a Flexible Manipulator Using an Iterative Learning Scheme," *IEEE Access* 7 (2019): 145934–145943.

32. Y. Chen, "Chuang Ch. Robust Control Design for a Class of Mismatched Coupled Uncertain Systems," *Optimal Control Applications and Methods* 18, no. 2 (1997): 83–107.

33. J. Xu, Y. Du, Y. H. Chen, H. Guo, and X. Ding, "Guaranteeing Uniform Ultimate Boundedness for Uncertain Systems Free of Matching Condition," *IEEE Transactions on Fuzzy Systems* 26, no. 6 (2018): 3479–3493.

34. Q. Sun, X. Wang, G. Yang, Y. H. Chen, and P. Duan, "Robust Pointing Control of Marching Tank Gun With Matched and Mismatched Uncertainty," *IEEE Transactions on Cybernetics* 52, no. 8 (2021): 7303–7318.

35. F. Zhai, Y. Yin, C. Li, W. Tian, and Z. Qiao, "Stiffness modelling and Feedforward Control of Servo Electric Cylinder Drive System," *Journal of Jilin University* 51 (2021): 442–449.

36. J. P. Den Hartog, *Mechanical vibrations* (Courier Corporation, 1985).